On the improvement of thermo-mechanical behavior of carbon/polyphenylene sulfide laminated composites upon annealing at high temperature

Benoît Vieille, E. Ernault, Nicolas Delpouve, J-D. Pujols Gonzalez, Antonella Esposito, Eric Dargent, L. Le Pluart, Laurent Delbreilh

Version of Record: https://www.sciencedirect.com/science/article/pii/S1359836821002493
Manuscript_54ac7d2521222f0d3bf9084fbabe316f

On the improvement of thermo-mechanical behavior of Carbon/polyphenylene sulfide laminated composites upon annealing at high temperature

B. Vieille[1], E. Ernault[1], N. Delpouve[1], J-D. Pujols Gonzalez[1], A. Esposito[1], E. Dargent[1], L. Le Pluart[2], L. Delbreilh[1]

[1] Normandie Univ, UNIROUEN Normandie, INSA Rouen, CNRS, Groupe de Physique des Matériaux - 76800 St Etienne du Rouvray, France

[2] Normandie Univ, ENSICAEN, UNICAEN, CNRS, Laboratoire de Chimie Moléculaire et Thioorganique - 14000 Caen, France

Address correspondence to: benoit.vieille@insa-rouen.fr

Abstract

This work consists in investigating the influence of the structural changes induced by annealing, such as the presence of a rigid amorphous fraction (RAF) and crosslinking, on the mechanical properties of polyphenylene sulfide (PPS) and the fracture mechanical behavior (particularly tenacity) of a Carbon/PPS laminated composite. The first part of the study aimed at obtaining PPS samples with different amounts of RAF, and in determining the conditions potentially favoring crosslinking. The results obtained on the matrix alone encouraged to transpose the mechanisms associated with the structural changes in PPS to the polymer phase in C/PPS laminated composites with woven-fibers reinforcement. The laminates have a [(+/-45°)]7 stacking sequence, whose overall mechanical response is controlled by the PPS matrix. The ultimate axial strength is little influenced (about 10% increase) by different annealing conditions with respect to as-received state. The optimum annealing conditions (230°C under air for 576 hours) contribute to the improvement of the axial stiffness (doubled compared to the as-received state). At the same time, the critical translaminar toughness (at initiation) is significantly increased (about 20%) and the translaminar failure is associated with a slower crack propagation.

Keywords: thermal ageing; thermoplastic; carbon fibers; toughness; translaminar failure

1. Introduction

One of the major concerns in aeronautics is to reduce the weight of planes in order to considerably reduce their kerosene consumption. One possible way to achieve a significant weight reduction of aeronautic structures is to replace metal pieces with composite pieces. Over the past forty years, composites have mostly consisted of thermoset matrices. However, thermosets have drawbacks (e.g. processability, recyclability) that thermoplastics can overcome. Even though thermoplastics are interesting materials for composite matrices, their impact resistance is not as good as metals'. For this reason, a special attention was paid to the investigation of the thermo-mechanical behavior of thermoplastics, with the aim of improving their damage tolerance and impact resistance. Among all the high-performance thermoplastics commonly considered for aeronautical applications, polyphenylene sulfide (PPS) is a thermostable semi-crystalline polymer that seems to be a good candidate as a thermoplastic matrix in carbon fiber reinforced composites [1].

Previous studies have been specifically devoted to evaluation of the influence of the conditions for thermal treatment on the fracture properties and mechanical behavior of composite materials consisting of a semi-crystalline PPS matrix [2-6]. Liu et al. [7] showed that the tensile properties and failure modes of carbon fiber reinforced PPS laminates subjected to isothermal heat treatments at different temperatures and exposure times are significantly affected by the crystallinity of the PPS matrix. In the temperature range of 100–210°C and for exposure times of 1–3 hours, it appeared that increasing the temperature and the exposure time results in an initial and gradual increase in both the degree of crystallinity and the tensile strength, followed by a decrease. Optimal values of the degree of crystallinity (about 65%) and the tensile strength (about 718 MPa) were obtained for a heat treatment corresponding to 150°C and 2 hours exposure. Compared to the as-received specimens, these values correspond to an increase of 46 % and 15%, respectively. Microscopic observations revealed that the tensile failure modes after 100°C and 150°C heat treatments are primarily dominated by fiber pull-out and fiber breakage, respectively. At 210°C, the

failure mode is mainly due to debonding and delamination. Based on a similar approach with respect to different degrees of crystallinity obtained with different cooling rates after thermo-compression, Batista et al. investigated the influence of crystallization on the mechanical and thermal properties of C/PPS laminates [8]. More specifically, their work attempted to correlate the morphology with the thermal and mechanical properties (compression, interlaminar shear stress, impact and interlaminar fracture toughness). For lower cooling rates, the degree of crystallinity increases and the same trend is observed for the compressive, interlaminar shear strengths, as well as impact resistance. End-notch flexure (ENF) tests also showed that the mode-II interlaminar fracture toughness is strongly influenced by the PPS degree of crystallinity, and lower cooling rates appeared to be responsible for stronger interfacial bonds. Ultimately, the mechanical properties of PPS-based laminates can be optimized by carefully selecting the cooling rate applied to the matrix during the processing cycle of the composite.

Therefore, improvement of the mechanical properties with the crystallinity dependence on annealing conditions was reported. To the authors' best knowledge, the impact of structural modifications in the amorphous phase at constant crystallinity, i.e., when the maximum degree of crystallinity has been reached, was, however, not investigated. In this study, it is proposed to tailor the mechanical properties of semi-crystalline Carbon/PPS laminated composites by inducing changes in the amorphous phase mobility. To reach this goal, samples were first crystallized at their maximum extent. Then, the annealing was prolonged with the aim of impacting the amorphous phase, either by inducing high contents of rigid amorphous fraction or by promoting crosslinking reactions.

1.1 Rigid amorphous fraction

The most conventional microstructural description of semi-crystalline polymers is done by a two-phase model consisting of a crystalline phase (X_c) and an amorphous phase (X_a). A two-phase model can be simply written as follows:

$$X_c + X_a = 1 \quad \text{(Eq. 1)}$$

However, sometimes the two-phase model fails to explain the behavior of semi-crystalline polymers [9]. In the 80's, Menczel and Wunderlich proposed a three-phase model [9-10] where the amorphous phase is divided into two fractions: one that devitrifies at the glass transition, i.e. the mobile amorphous fraction (MAF), and one that devitrifies at higher temperatures, i.e. the rigid amorphous fraction (RAF). The latter would be responsible for the coupling between the crystalline domains and the MAF. This description can be formalized as follows:

$$X_{MAF} + X_{RAF} + X_C = 1 \quad \text{(Eq. 2)}$$

PPS has already been described with a three-phase model [11]. It was also shown that RAF could significantly influence the mechanical properties of semi-crystalline polymers, such as polyamide 6, poly(ethylene terephthalate), and poly(L-lactic acid) [12-14]. In order to optimize the mechanical properties of PPS-based composite materials, it is therefore necessary to investigate the formation of RAF. The RAF content in a polymer can be modified by annealing, i.e. maintaining the sample at relatively high temperature for different durations.

1.2 Crosslinking reactions

In a semi-crystalline polymer subjected to thermal ageing, the amorphous and crystalline phases do not oxidize in the same way [3]. The less compact amorphous phase allows oxygen to penetrate within the macromolecular structure, thus facilitating chemical reactions. In some cases, these reactions modify the crystallinity degree of the polymer [4]. The crystalline phase, which is more stable and denser, is more difficult to oxidize. On the other hand, it is more resistant, stiffer, and exhibits a more brittle behavior with respect to the amorphous phase. If the thermal ageing modifies

the morphology of the crystalline phase, one may observe a degradation of the mechanical properties of the polymer. In some other cases, the oxidization leads to crosslinking reactions, increasing both the glass transition temperature and the rigidity. The crosslinking degree increases with the duration of exposure to high temperatures, implying a rearrangement and deep modification of the amorphous phase eventually leading to the creation of a 3-dimensional network.

1.3 Objectives of the study

In this study, the annealing conditions favorable to the formation of RAF, either alone or in combination with crosslinking were determined. C/PPS laminates were then annealed to foster both the formation of RAF and the crosslinking in order to evaluate their possible influence on the tensile properties (axial stiffness, ultimate strength and strain at failure), but also on the fracture behavior and the corresponding translaminar fracture toughness. The ultimate objective of this work was to examine if the mechanical changes observed in the PPS resin alone are transposable to C/PPS laminated composites. The mechanical tests on the composites were conducted at 120°C on angle-ply $[(+/-45°)]_7$ laminates, whose overall mechanical response is controlled by the matrix. A testing temperature of 120°C was purposely chosen to be representative of a service temperature in the surroundings of an aircraft engine.

2. Materials and experimental set-up

2.1 Materials

The investigated laminates are composite samples consisting of a PPS matrix reinforced with carbon fibers [15]. The reinforcement is a balanced fabric with a satin pattern of 5 (T300 3K 5HS, Toray). The resin was supplied by Ticona (Fortron 0214). The volume content of the components is 50%, which corresponds to a matrix mass content of 42%. The manufacture of 7-ply laminates with an angle ply [±45]7 stacking sequence allows obtaining samples with a tensile mechanical response

driven by the matrix shear behavior because of the presence of many matrix-rich regions within the laminates (Fig. 1). The characteristic temperatures of these C/PPS laminates determined from modulated-temperature DSC [15-16] are T_g = 95°C for the glass transition temperature and T_m = 235°C for the melting temperature.

2.2 Annealing conditions

C/PPS specimens were placed in a primary vacuum furnace at different annealing temperatures (115°C and 230°C) and for different times (20h, 576h, 1417h). Only annealing at 230°C was carried out under two atmospheres (air and vacuum). These annealing conditions are summarized in Table 1.

2.3 Experimental protocol

2.3.1 Fast scanning calorimetry (FSC)

Fast scanning calorimetry (FSC) analyses were performed at 1500 K s^{-1} under a 20 mL min^{-1} nitrogen flow in Flash DSC 1 (Mettler Toledo) equipped with a Huber TC100 intra-cooler. The samples were positioned on MultiSTAR UFS 1 MEMS chip sensor. Calibration was done using Mettler Toledo standard protocol. Samples were annealed at different temperatures between T_g and T_m. The samples were first melted at 350 °C, then cooled down to the crystallization temperature, held in isothermal conditions, and finally cooled down to −60 °C. The subsequent heating scan from -60 to 350 °C allowed calculating X_c, X_{MAF} and X_{RAF}. The rate used for the heating and cooling ramps was 1500 K s^{-1}. Before any crystallization procedure, it was checked that a cooling rate of 1500 K s-1 was sufficient to inhibit the crystallization of PPS when it was not annealed. The procedure used to calculate X_c and X_{RAF} in PPS has been fully described in the reference [17]. It is not detailed there as it is beyond the scope of the study.

2.3.2 Swelling experiments

To evidence the possibility of crosslinking reactions, gravimetric measurements were performed consecutive to swelling in chloroform. The water uptake (WU) of PPS sample, which corresponds to the ratio between the gain of mass and the mass of dried sample, was followed as a function of the immersion time, following the same procedure as Yang et al. [18]. The experiments were reproduced ten times at least then the average value was recorded.

2.3.3 Dynamic mechanical analysis (DMA)

The evolution of the mechanical properties of the pure PPS with different RAF contents was evaluated by performing the DMA tests in a DMA Q800 (TA instruments) using rectangular samples (35 x 12 x 2 mm) adapted to a double-embedded bending stress. Temperature sweeps were performed from 28°C to 250°C at a heating rate of 2 $K.min^{-1}$ with an amplitude of 15 µm and a frequency of 1 Hz.

2.3.4 Monotonic tensile testing

The characterization of the mechanical behavior at high temperature was carried out using a uniaxial servo-hydraulic MTS machine equipped with hydraulic grips and a 100 kN force cell. The tensile tests were performed at 120°C using a thermal enclosure. The specimens were cut by water jet from 600x600mm^2 2.2 mm thick plates, according to two geometries corresponding to specific loading conditions, i.e. tensile test (Fig. 2a) and Compact Tension (CT) translaminar toughness test (Fig. 2b). Three specimens were tested in each configuration.

2.3.5 Estimation of fracture toughness at initiation and propagation

In thin laminates specimens, a plane stress state is prevalent. The ASTM-E1922 standard was used here to compute the translaminar fracture toughness of composites laminates whose fracture behavior is elastic-ductile [20]. This standard provides recommendations on specimen geometry for

estimating the translaminar fracture toughness of composite materials (Eccentrically loaded Single-Edge-notch Tensile), the use of standards derived from metallic materials is widely used for composite materials. Finally, there is no strict recommendation done by the standard on the specimen's thickness. As $[(+/-45°)]_7$ C/PPS laminates are characterized by a ductile fracture behavior (particularly at high temperature), their fracture behavior was quantified by means of the J-integral vs. crack growth resistance (J-R) curve, in order to assess the structural integrity of the material in the presence of preexisting defects [1]. These curves represent the energy per unit of fracture area required to initiate and propagate the crack. The value of the fracture toughness at the initiation is called J_{Ic} and is associated with the mechanical energy required for the fracture to occur in the material [19]. The procedure for obtaining the J-R curve is described in ASTM E1922 standard test method [20]. Depending on the fracture mode, the standard recommends the use of specimens with different geometries on which are machined notches for stress concentration and crack initiation purposes. Thus, fracture toughness tests were done on compact tension (CT) specimens whose dimensions are given in Figure 2. Four specimens were tested in each configuration. CT specimens have a ratio $\mathrm{a/w} = 0.45$. The critical translaminar toughness (at crack initiation) in mode I is classically estimated from this ratio and the stress intensity factor K_{Ic} [21]:

$$K_{Ic} = \frac{P_c}{t\sqrt{w}} . F(a/w) \qquad \text{(Eq. 3)}$$

Where P_c is the load applied to the specimen (the one measured by the cell force) at crack initiation, t is the sample thickness, $\boldsymbol{w}$ is the distance from the load line to the right edge of the specimen (Fig. 2b), $\boldsymbol{a}$ is the initial crack length and $\mathrm{F(a/w)}$ is a geometric correction function defined by the following relationship in the case of CT specimens:

$$\mathrm{F(a/w)} = \frac{2 + \mathrm{a/w}}{(1 - \mathrm{a/w})^{3/2}} [0{,}086 + 4{,}64.\,\mathrm{a/w} - 13{,}32.\,(\mathrm{a/w})^2 + 14{,}72.\,(\mathrm{a/w})^3 - 5{,}6.\,(\mathrm{a/w})^4] \qquad \text{(Eq. 4)}$$

In materials with ductile fracture behaviors, the fracture toughness J during propagation is computed from the elastic-plastic fracture mechanics concepts [22-26]:

$$J = J_{elastic} + J_{plastic} \quad \text{(Eq. 5)}$$

With $J_{elastic}$ computed from the mode I critical stress intensity factor K_{Ic} and the elastic constants of the elementary ply in orthotropic composite materials [20]:

$$J_{elastic} = C_I . K_{Ic}^2 \quad \text{(Eq. 6)}$$

with $C_I = \sqrt{\frac{1}{2E_xE_y}}\sqrt{\sqrt{\frac{E_x}{E_y}} - \nu_{xy} + \frac{E_x}{2G_{xy}}}$ in plane-stress conditions, where E_x, E_y, G_{xy} and ν_{xy} are the in-plane mechanical properties of the equivalent orthotropic material.

The plastic component $J_{plastic}$ is obtained from the dissipated mechanical energy A_{pl} corresponding to the area under the force-displacement curve:

$$J_{plastic\,(i)} = \left[J_{plastic\,(i-1)} + \frac{\eta_{pl\,(i-1)}}{b_{(i-1)}}\left(\frac{A_{pl\,(i)} - A_{pl\,(i-1)}}{B_N}\right)\right] . \left[1 - \gamma_{pl\,(i-1)}\left(\frac{a_{(i)} - a_{(i-1)}}{b_{(i-1)}}\right)\right] \quad \text{(Eq. 7)}$$

where $\eta_{pl\,(i-1)} = 1.9$ and $\gamma_{pl\,(i-1)} = 0.9$ in agreement with the ASTM E1922 standard test method in the case of CT specimens [20], B_N is the net specimen thickness, $a_{(i)}$ and $b_{(i)} = w - a_{(i)}$ are the crack length and the unbroken ligament at iteration (i), respectively. These values are computed for each iteration (i) by means of experimental data obtained from digital image analyses detailed in the next section (see Fig. 3).

2.3.6 In-situ location of the crack tip

A high-speed monochrome Grasshopper® camera was used to record digital images during thermo-mechanical loading. The VIC-2D digital image correlation software obtained the confidence field associated with the convolution factor (sigma indicator) of each pattern in the region of interest. By means of an algorithm based on a binarization method and implemented in the free source

numerical computation software Scilab, the digital images were thresholded in order to track the location of the crack tip during mechanical loading (Fig. 3). To know the position of the crack edges, images are computed by the algorithm from top to bottom in search of a pixel value change, therefore indicating the edge of the crack. The obtained position is then compared with the previous position to ensure that the new crack tip is not too far away to avoid artefact effects. The physical meaning of the crack tip is also verified by comparing its location between two successive images.

3. Results and discussion

3.1 Quantification of the RAF in PPS specimens (pure matrix)

Fast scanning calorimetry study dealing with the formation of RAF in PPS (Figure 4) provided the best conditions of thermal treatment to enrich PPS samples with RAF, i.e. between 115°C and 230°C [15]. This is essential to assess whether the RAF formed in PPS alone has an influence on its mechanical properties (and by extension on those of a C/PPS composite) or not [16]. In addition, annealing temperatures unfavorable to the formation of RAF have been identified (235 and 243 °C) allowing to approach a two-phase model (See Eq.1 and the line $X_{MAF} + X_c = 100\%$ in Figure 4). Indeed, the data divergence from a two-phase model is a proof of RAF formation whereas the data alignment on the line $X_{MAF} + X_c = 100\%$ proves that RAF does not form. At 115°C and 230°C, the RAF content increases as the annealing time increases.

3.2 Combination with crosslinking in thermo-oxidizing conditions

According to Figure 5, similar values of WU were obtained after annealing at 115 °C under vacuum as compared to pristine PPS (as-received) at high immersion times, but the increase in WU is delayed, probably due to the RAF. After annealing at 230 °C, the curve quickly reaches a plateau highlighting a clear decrease of WU, which is further aggravated when the annealing is performed under air instead of vacuum. The decrease of WU at high immersion time shows that the PPS

structure limits its water absorption capability. It should be related to an increase in the crosslinking density due to chemical reactions occurring at high annealing temperatures.

3.3 DMA results

When the annealing time at 115 °C increases (Fig. 6a), the mechanical signature of the glass transition, i.e., the drop of storage modulus, shifts towards high temperatures. This is in agreement with the results obtained by calorimetric analyses (modulated-temperature DSC, fast scanning calorimetry) revealing an increase in the glass transition temperature for increasing annealing times [15]. In addition, the loss factor signal (Tan delta) shows a clear decrease in amplitude and a widening of the peak associated with the glass transition as a function of the annealing time. It is worth noticing that X_c remains relatively constant for the different annealing conditions (about 40%). It is therefore possible to attribute the changes observed by DMA to an increasing X_{RAF}. Increasing the annealing time at 230 °C (Fig. 6b) has the same consequences, with the difference that the shift and broadening of the glass transition becomes spectacular. This is characteristic of crosslinking chemical reactions [27], which occur concomitantly with the RAF formation. Moreover, an increase in the storage modulus with the annealing time is also observed at room temperature, which, as previously reported [28], agrees with the decrease in WU (Fig. 5).

3.4 Monotonic tensile behaviour

The increase in temperature and annealing time makes the macroscopic tensile behavior of the C/PPS laminates less ductile (Fig. 7), with a decrease in the axial strain at failure (-52% when the samples annealed at 230°C for 576h are compared to pristine samples). It is assumed that the formation of RAF within the PPS matrix results in lower macromolecular mobility, hence suggesting that the plasticity of the PPS matrix is reduced by the annealing conditions. The tensile

response of $[(+/-45°)]_7$laminates is known to be driven by the PPS matrix shear behavior along with the rotation of carbon fibers bundles. This structural effect is directly correlated to the plastic deformation of the PPS matrix in the matrix-rich regions of woven-ply [±45]7 laminates (as shown in Fig. 1). This deformation mechanisms and this structural effect cause necking that is clearly observable on the C/PPS stress–strain curves, as well as on the failed specimens. Necking comes along with an important delamination, resulting in lower ultimate strength [29-30]. Thus, the ultimate axial strength is little influenced (about 10% increase) by different annealing conditions with respect to as-received state (Fig. 8). Thermal ageing also contributes to a significant stiffening of the material, with an increase of about 100% in axial stiffness.

3.5 Translaminar failure behavior and fracture toughness

The effects of different annealing conditions on the PPS matrix are expected to affect the failure mechanisms and the evolution of the critical toughness in mixed mode (stacking sequence $[(+/-45°)]_7$). The measurements of critical toughness were obtained from Equations (3-4) applied to the force-displacement data (Figs. 9-10-11) relating to the tensile behavior of CT specimens. At room temperature, the fracture behavior is quasi-brittle for all test configurations. At 120°C, the response becomes elastoplastic in the first phase of loading and then quasi-brittle after initiation of fracture. The increase in the test temperature from room temperature to 120 °C results in a significant decrease (from -20 to -40%) in the stress corresponding to the failure of the first bundle of fibres, which also occurs for higher imposed displacement (Fig. 9). It can also be pointed out that the propagation of the translaminar crack is stable in all cases.

Fig. 10 shows the influence of the annealing time on the fracture behavior when the test is performed at 120°C, which is the typical operating temperature for composites in an aircraft engine nacelle. Annealing at 115°C (i.e. slightly above the glass transition temperature), which is known to favor the formation of RAF in the PPS matrix alone, also contributes to a small increase in the

stiffness and ultimate stress at break, a phenomenon already observed in C/PPS laminates [3]. In addition, when annealing at 230°C (i.e. slightly below the melting temperature), the increase in the annealing time is accompanied by a significant increase in the axial stiffness and ultimate tensile strength (+25%). This is attributed to the possible combination of RAF and crosslinking.

The mode I critical fracture toughness $J_{Ic} = J_{elastic}$ is computed from the experimental data using Eqs. 3-4 and Eq. 6. The influence of the annealing conditions on the fracture behavior can also be evaluated based on the observations of both the macroscopic fracture response (Fig. 11) and the mode I critical fracture toughness J_{Ic} (Fig. 12). For a short annealing time (e.g. 20h), the annealing temperature has little influence on the mechanical response. In order to evaluate the possible influence of the annealing atmosphere, conditions favoring crosslinking in addition to the formation of RAF (230 °C during 576h) were chosen. Compared to the as-received samples, the C/PPS laminates annealed under air show an improvement in mechanical properties and critical fracture toughness at initiation (about +22%). On the other hand, the C/PPS laminates annealed under vacuum showed a 27% decrease in the mode I critical fracture toughness (Fig. 12). The best annealing conditions for improving the mechanical properties and the fracture toughness of C/PPS laminates are therefore an increased annealing time (576h), an annealing temperature close to 230°C, and an oxidizing atmosphere. The first breakage of fibre bundles occurs at similar levels of imposed displacement but at higher levels of mechanical load. It is worth reminding that in an oxidizing atmosphere the crosslinking reactions in the amorphous phase occur in higher proportions. Therefore, the stiffness and critical fracture toughness seem to decisively benefit from crosslinking.

The fracture surfaces observed in the different test configurations are similar. This suggests that the influence of the annealing conditions, clearly visible on the properties (stiffness, strength, fracture toughness) and the overall mechanical response, does not translate into macroscopic cracking, as the translaminar crack follows an identical path imposed by the areas of overlap (Fig. 13). However,

the differences in the fracture behavior, and in particular in the I-mode toughness (+60%), observed between the as-received C/PPS laminates and after annealing at 230°C for 576 hours under air, can be analyzed more closely using the crack front monitoring technique previously introduced. It appears that the first fibre breakage occurs at almost the same applied displacement (Fig. 14).

However, the crack grows at the first fibre breakage (very slight drop in load) in the C/PPS annealed at 230°C, whereas the crack growth starts later in the as-received specimen. The gradual breakage of the fibre bundles comes along with a drop in the mechanical load borne by the specimen and by "jumps" in the length of the crack, reflecting the redistribution of the load by the neighbouring undamaged fibres. During crack propagation, and for a given applied displacement, the crack is longer (5mm on average) in the as-received specimen, confirming that the overall mechanical properties of the C/PPS laminates are improved by the formation of RAF in combination with crosslinking. It also suggests that the enhanced fracture toughness of C/PPS after being annealed at 230°C under air for 576 hours is associated with a slower crack propagation.

The J-R curves can be drawn from an estimation of both the strain energy release rate (obtained from the computation of the experimental data according to Eqs. (3-7) and the crack length (based on digital image analysis, see section 2.2.6) (Figure 15). In agreement with the results previously presented in Fig. 12, the mode I critical fracture toughness J_{Ic} (corresponding to crack initiation) is about 20% higher in the C/PPS specimens annealed at 230°C during 576h. From the crack propagation standpoint, the change in the strain energy release rate is similar in both specimens, i.e. before and after annealing, suggesting that the structural changes resulting from specific annealing conditions only significantly influence the initiation of the translaminar crack. In other words, once the crack is initiated, the energy required to grow the crack is the same.

4. Conclusions

This study investigated the influence of the annealing conditions applied to C/PPS laminated composites, combining a PPS matrix and a woven carbon fibre reinforcement, with a $[+/-45°]_7$ stacking sequence (whose mechanical response is driven by the matrix) on the mechanical properties. Annealing conditions (temperature, time, and atmosphere) that are favorable to both the formation of RAF and crosslinking, obtained in a preliminary calorimetric study carried out on the PPS matrix alone, were imposed on laminated composites. Mechanical loads in tensile and compact tensile modes (providing mode I fracture toughness) were applied at a temperature of 120°C (corresponding to the typical service temperature in an aircraft engine nacelle).

The results suggested that it is possible to design the mechanical properties of laminated composites to specific requirements by playing both on RAF formation and crosslinking reactions. When annealing is performed at 115 °C, the formation of RAF induces a slight increase in the stiffness while keeping an acceptable value of the strain at failure. The optimum annealing conditions (230°C under air for 576h) allowing a combination of RAF formation and crosslinking proved to be the most favorable for improving the axial stiffness of the mechanical composite (twice the value of the as-received specimens), and resulted in a significant increase (about 20%) in the critical translaminar fracture toughness. From the crack propagation standpoint, the changes in the strain energy release rate are similar in both samples (as-received and annealed), suggesting that the structural changes resulting from specific annealing conditions have a significant influence only on the initiation of the translaminar crack. Once the crack is initiated, the energy required to grow the crack is the same in all the specimens, regardless the annealing conditions. In the optimum annealing conditions, the translaminar failure is associated with a slower crack propagation.

Acknowledgments

The work presented in this study is the result of the project RIN (Réseau d'Intérêt Normand) FARM (Influence de la Fraction Amorphe Rigide sur les propriétés Mécaniques et physiques des

polymères semi-cristallins: contexte aéronautique) funded by the Normandy region. The authors would like to thank Léa Monnier and Joicy Dos Santos Cordovil for their contribution to the investigation of the matrix properties.

References

[1] Vieille, B., Gonzalez, J. D., & Bouvet, C. (2018). Fracture mechanics of hybrid composites with ductile matrix and brittle fibers: Influence of temperature and constraint effect. Journal of Composite Materials 53(10), 1361-1376.

[2] Scobbo J.J., Hwang C.R. Annealing effects in Poly(Phenylene Sulfide) as observed by dynamic mechanical analysis. Polymer Eng. and Sci. 34(23), 1744-1749 (1994).

[3] Lee T.H., Boey F.Y.C & Loh N.L. Characterization of a fiber-reinforced PPS composite by dynamic mechanical analysis: effect of aspect ratio and static stress. Composite Sci. and Tech 49, 217-223 (1993).

[4] Pantelakis S.G., Katsiropoulos C.V., Lefebure P. Effect of thermal treatment on the tensile and in-plane shear behavior of carbon fiber-reinforced poly(phenylene sulfide) composite specimens. Journal of Applied Polymer Sci. 107, 3190–3199 (2008).

[5] Zuo P. Etude de l'effet du vieillissement thermique sur le comportement en fatigue du composite de poly (sulfure de phénylène) renforcé par des fibres de verre (PPS/FV). Thèse de Doctorat ENSAM-Paris Tech (2018).

[6] Zuo P.,Fitoussi J., Shirinbayan M, Bakir F, Tcharkhtchi A. Thermal aging effects on overall mechanical behavior of short glass fiber-reinforced polyphenylene sulfide composites. Polymer Eng. and Sci. 59(4), 765-772 (2019).

[7] Y. Liu, X. Zhou, Z. Wang. Effect of isothermal heat treatment on crystallinity, tensile strength and failure mode of CF/PPS laminate. High performance polymer, doi: 10.1177/0954008320969843 (2020).

[8] N.L. Batista, K. Anagnostopoulos, E. Cocchieri Botelho, H. Kim. Influence of crystallinity on interlaminar fracture toughness and impact properties of polyphenylene sulfide/carbon fiber laminates. Engineering Failure Analysis 2021, 119: 104976.

[9] Menczel, J. & Wunderlich, B. Heat capacity hysteresis of semicrystalline macromolecular glasses. J. Polym. Sci. Polym. Lett. Ed. **19**, 261–264 (1981).

[10] Wunderlich, B. Reversible crystallization and the rigid–amorphous phase in semicrystalline macromolecules. Prog. Polym. Sci. **28**, 383–450 (2003).

[11] Huo, P. & Cebe, P. Effects of thermal history on the rigid amorphous phase in poly(phenylene sulfide). Colloid Polym. Sci. **270**, 840–852 (1992).

[12] Kolesov I. & Androsch R. The rigid amorphous fraction of cold-crystallized polyamide 6. Polymer 53, 4770-4777 (2012).

[13] Rastogi R., Vellinga W. P., Rastogi S., Schick C. & Meijer H.E.H. The three-phase structure and mechanical properties of poly(ethylene terephthalate). J. Polym. Sci. Part B Polym. Phys. 42, 2092–2106 (2004).

[14] Aliotta L., Gazzano, M., Lazzeri, A., Righetti M.C. Constrained Amorphous Interphase in Poly(l-lactic acid): Estimation of the Tensile Elastic Modulus. ACS Omega, 5, 20890–20902 (2020).

[15] Ernault E., Delpouve N., Vieille B. Influence de la fraction amorphe rigide sur les propriétés mécaniques d'un composite Carbone/poly(phenylene sulfide). 28ème colloque national Déformation des Polymères solides, La Bresse, France, 25-28 septembre 2018.

[16] Ernault E., Vieille B., Delpouve N., Pujols-Gonzalez J-D. Influence de la fraction amorphe

rigide sur le comportement à rupture de composites Carbone/PPS. Journées Nationales des Composites JNC21, Bordeaux INP, France, 1-3 Juillet.

[17] Fosse C., Bourdet A., Ernault E., Esposito A., Delpouve N., Delbreilh L., Thiyagarajan S., Knoop Rutger J.I., Dargent E. Determination of the equilibrium enthalpy of melting of two-phase semi-crystalline polymers by fast scanning calorimetry. Thermochimica Acta, Volume 677, 67-78 (2019).

[18] L.-Q. Yang, B. He, S. Meng, J.-Z. Zhang, M. Li, J. Guo, Y.-M. Guan, J.-X. Li, Z.-W. Gu. Biodegradable cross-linked poly(trimethylene carbonate) networks for implant applications: Synthesis and properties. Polymer 2013, 54, 2668.

[19] Begley J.A., Landes J.D. The J-integral as a fracture criterion. ASTM STP 514,1972:1–20.

[20] ASTM E1922 − 15, Standard Test Method for Translaminar Fracture Toughness of Laminated and Pultruded Polymer Matrix Composite Materials (2015).

[21] Tada H, Paris PC, Irwin GR. The stress analysis of cracks handbook. Third edition. January: ASME Press; 2000.

[22] Rice JR, Paris PC, Merkle JG. Some further results of J-integral analysis and estimates. Progress in flaws growth and fracture toughness testing, ASTM STP 536,1973:231–45.

[23] Sumpter JDG, Turner CE. Method for laboratory determination of Jc. Cracks and fracture. ASTM STP 601, 1976:3–18.

[24] Turner CE. The ubiquitous ηfactor. Fracture mechanics: twelfth conference. ASTM STP 700. American Society for Testing and Materials; 1980. p. 314–37.

[25] Roos E, Eisele U, Silcher H. A procedure for the experimental assessment of the Jintegral by means of specimen of different geometries. Int J Press VesPip, 1986;23:81–93.

[26] Turner CE. Fracture toughness and specific energy: a reanalysis of results. Mater Sci Eng 1973; 11:275–82.

[27] Zuo, P., Tcharkhtchi A., Shirinbayan M., Fitoussi J., Bakir F. Effect of thermal aging on crystallization behaviors and dynamic mechanical properties of glass fiber reinforced polyphenylene sulfide (PPS/GF) composites. J. Polym. Res. 27, 77 (2020)

[28] S. Araujo, F. Batteux, W. Li, L. Butterfield, N. Delpouve, A. Esposito, L. Tan, J.-M. Saiter, M. Negahban. A structural interpretation of the two components governing the kinetic fragility from the example of interpenetrated polymer networks. Journal of polymer science, part B: polymer physics 2018, doi: 10.1002/polb.24722.

[29] B. Vieille, L. Taleb. About the influence of temperature and matrix ductility on the behavior of carbon woven-ply PPS or epoxy laminates: Notched and unnotched laminates. Composites Science and Technology, Volume 71, Issue 7, 2011, Pages 998-1007.

[30] B. Vieille, J. Aucher, L. Taleb. Comparative study on the behavior of woven-ply reinforced thermoplastic or thermosetting laminates under severe environmental conditions. Materials & Design, Volume 35, 2012, Pages 707-719.

Figures captions

Fig. 1 – Optical microscope through-the-thickness observations of PPS matrix-rich regions in C/PPS angle-ply $[\pm 45]_7$ laminates

Fig. 2 – Geometry of tensile specimens allowing the characterization of the fracture behavior of C/PPS laminates: (a) monotonic tensile test - (b) Compact Tension translaminar toughness test [5]

Fig. 3 – Illustration of the in-situ location of the crack tip by means on a binarization algorithm applied to digital images

Fig. 4 – Evolution of the RAF content in PPS annealed at different temperatures [15]

Fig. 5 – Degree of swelling in weight percentage as a function of the immersion time in chloroform for as-received and annealed PPS samples

Fig. 6– Influence of the annealing time on the storage modulus and the loss factor for PPS samples annealed under air at (a) 115 °C and (b) 230°C

Fig. 7 – Influence of the annealing conditions on the tensile mechanical response of C/PPS laminates at 120°C: (a) Annealed at 230°C under air for different durations - (b) Annealed under air for 576 hours at different temperatures

Fig. 8 – Influence of the annealing conditions under air on the mechanical tensile properties of C/PPS laminates at 120°C: (a) axial stiffness, (b) ultimate axial strength, and (c) strain at failure

Fig. 9 – Influence of the testing temperature (room temperature noted RT and 120°C) on the fracture behavior of (a) the as received C/PPS laminates, and C/PPS laminates respectively annealed under air at (b) 115 °C during 20 and 1417 hours and (c) 230 °C during 20 and 576 hours. Annealing at 230 °C for 576h was done under air and vacuum.

Fig. 10 – Influence of the annealing time (ranging between 20h and 1471h) under air on the fracture behavior at 120°C of C/PPS laminates annealed at (a) 115 °C and (b) 230 °C

Fig. 11 – Influence of (a) the annealing temperature (115°C and 230°C) and (b) the atmosphere on the fracture behavior of C/PPS laminates tested at 120°C

Fig. 12 – Influence of the annealing conditions on the mode I critical fracture toughness $\mathbf{J_{Ic}}$ (at initiation) of angle-ply C/PPS laminates at 120°C

Fig. 13 – Influence of annealing temperature on the mode I toughness of C/PPS laminates annealed in conditions favoring a combination of RAF formation and crosslinking

Fig. 14 – Comparison of a C/PPS laminated sample before and after annealing at 230°C under air for 576 hours: evolution of crack length as a function of displacement.

Fig. 15 – J-R curve representing the evolution of the strain energy release rate as a function of the crack length for as-received C/PPS specimens and their homologues annealed at 230 °C under air during 576h

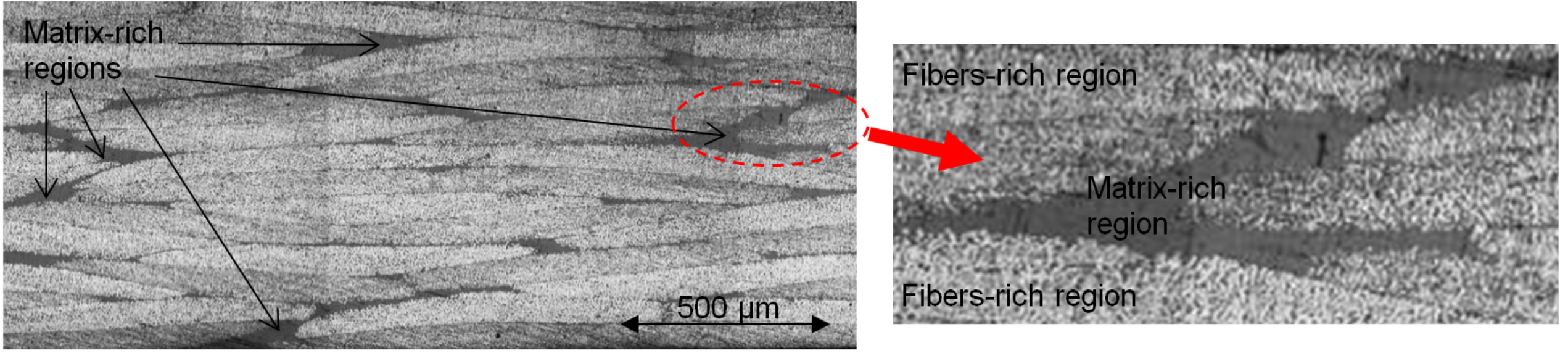
Matrix-rich
regions
500 µm
Fibers-rich region
Matrix-rich
region
Fibers-rich region

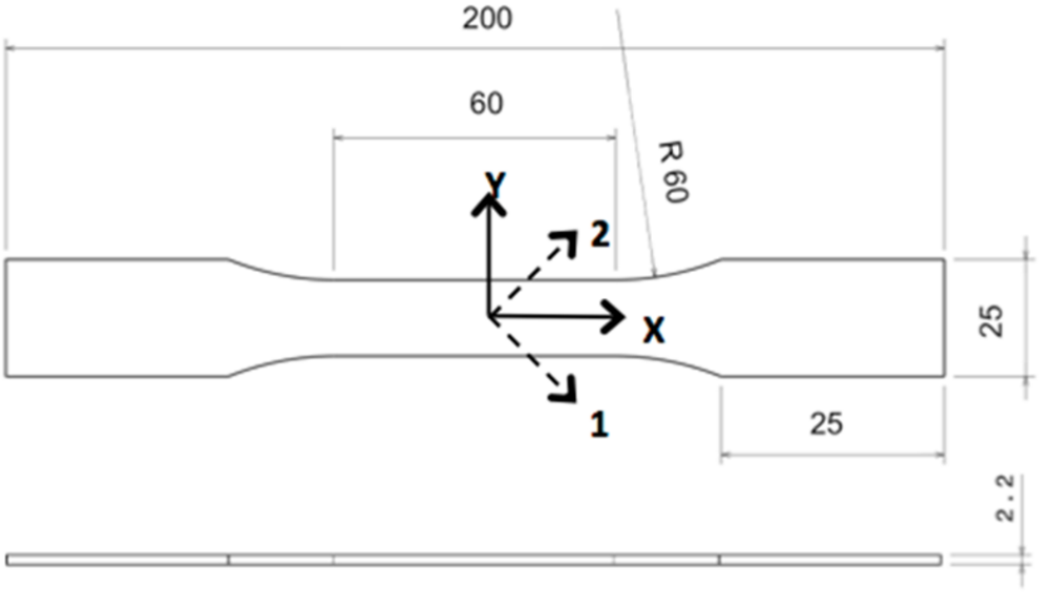
200
60
R 60
Y
2
X
1
25
25
2.2

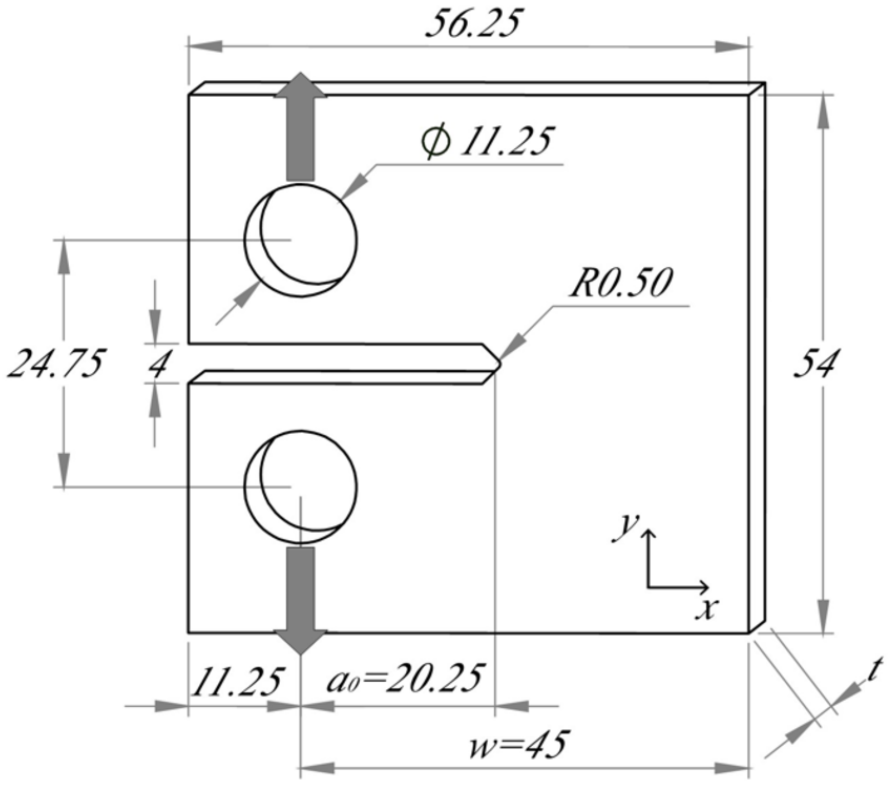
56.25
ϕ 11.25
R0.50
24.75
4
54
y
x
11.25
a₀=20.25
w=45
t

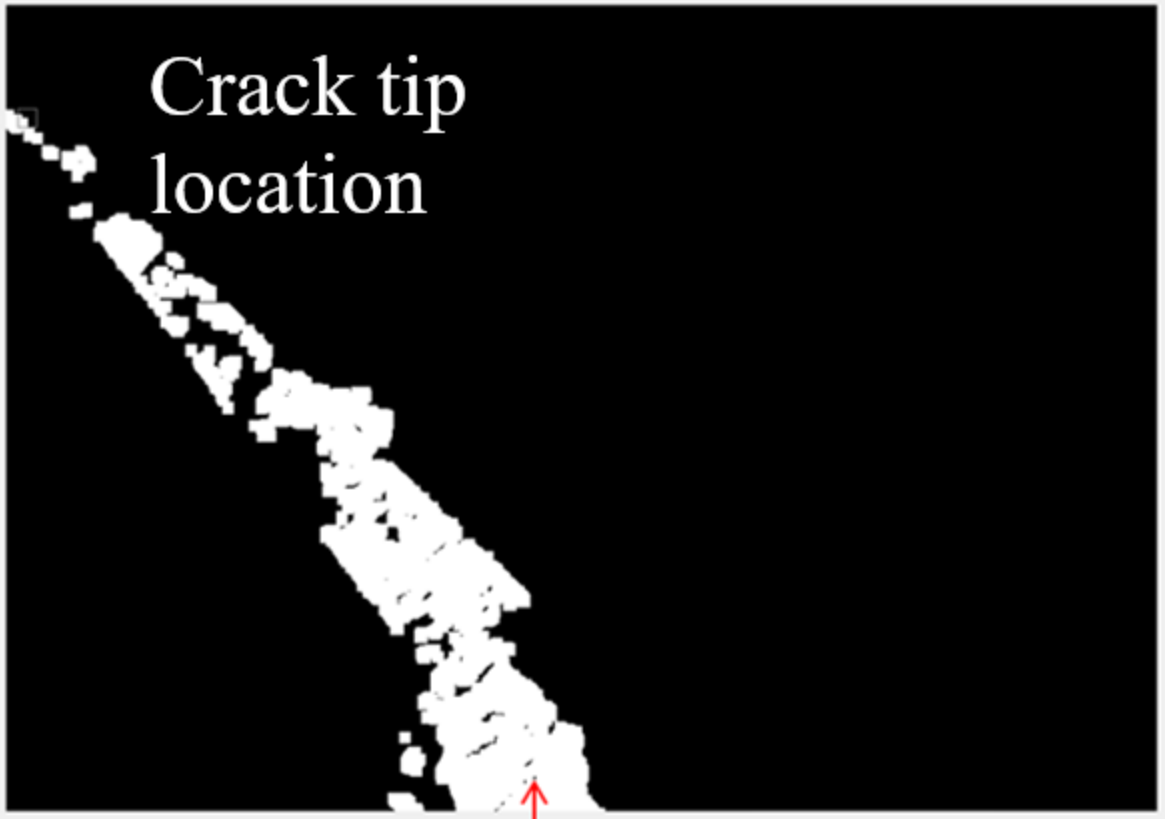

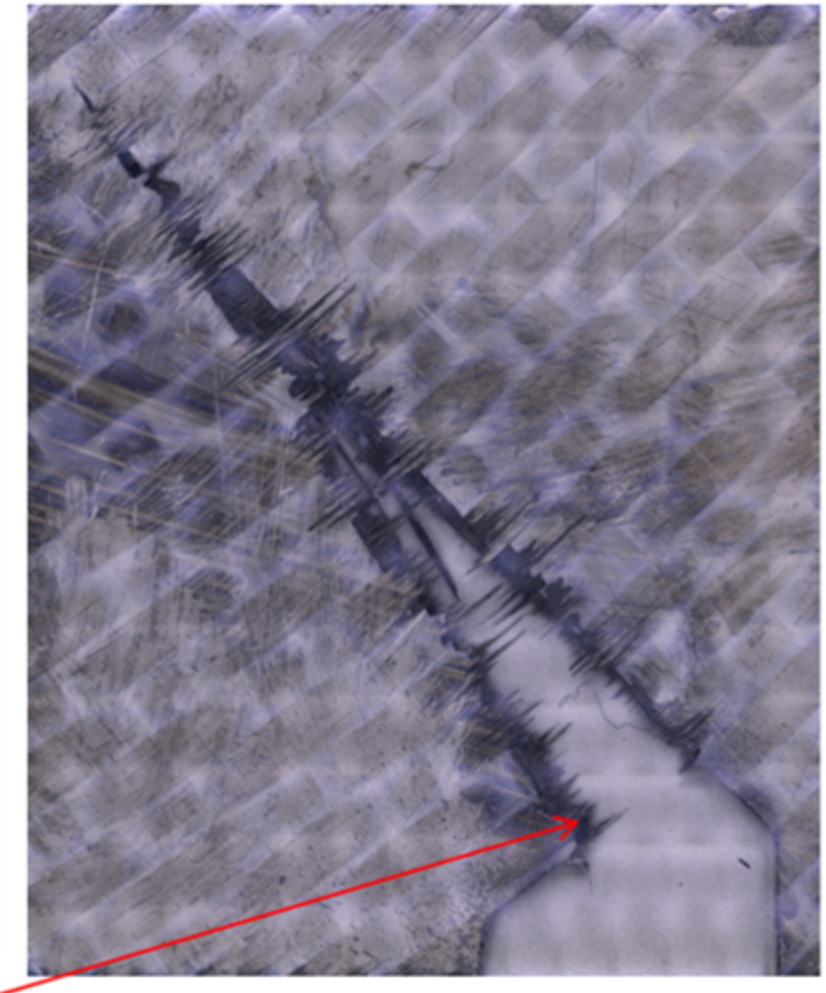

Front of initial
machined notch

2mm

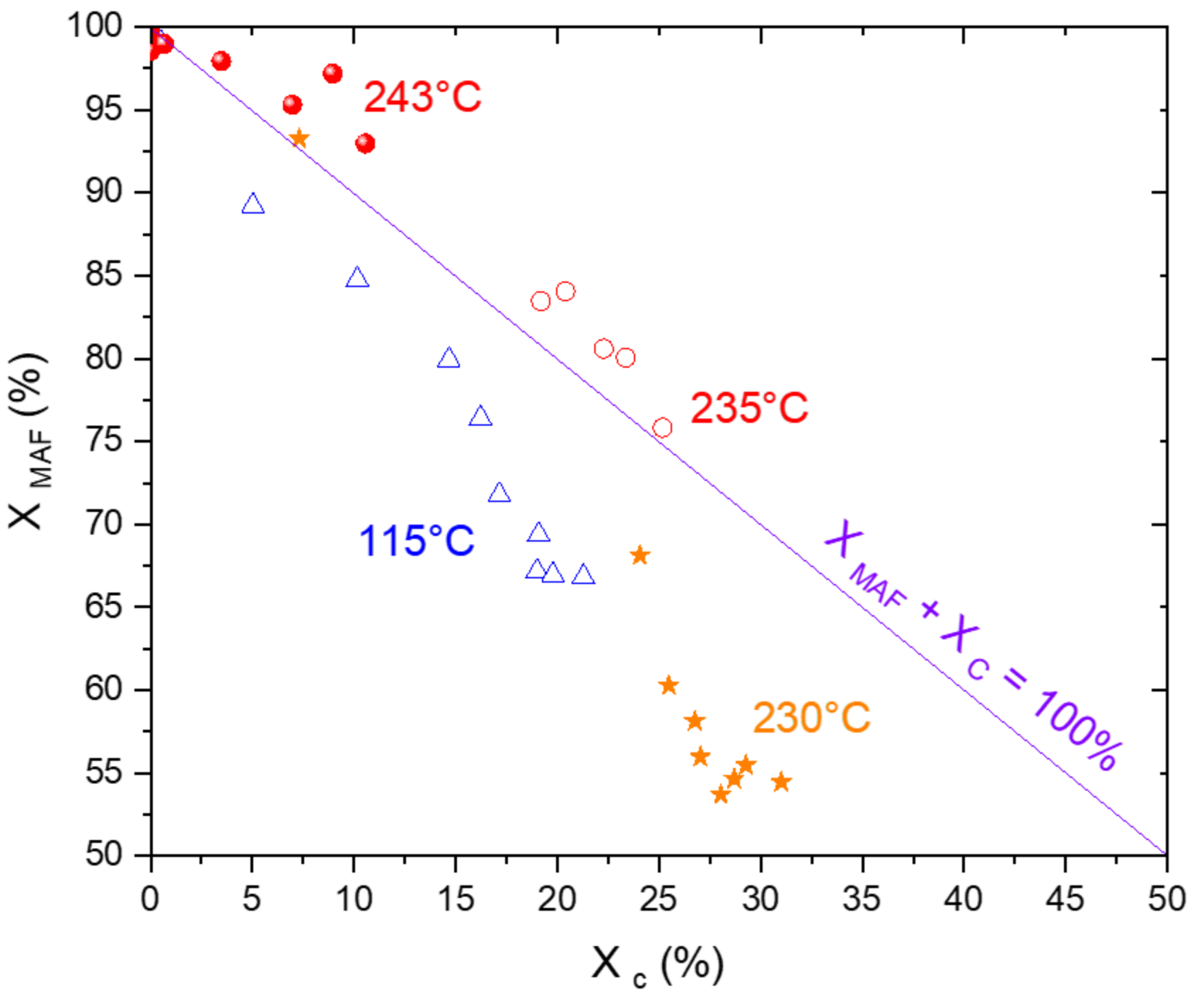
243°C
235°C
115°C
230°C
$X_{MAF} + X_C = 100\%$
X_{MAF} (%)
X_c (%)
100
95
90
85
80
75
70
65
60
55
50
0
5
10
15
20
25
30
35
40
45
50

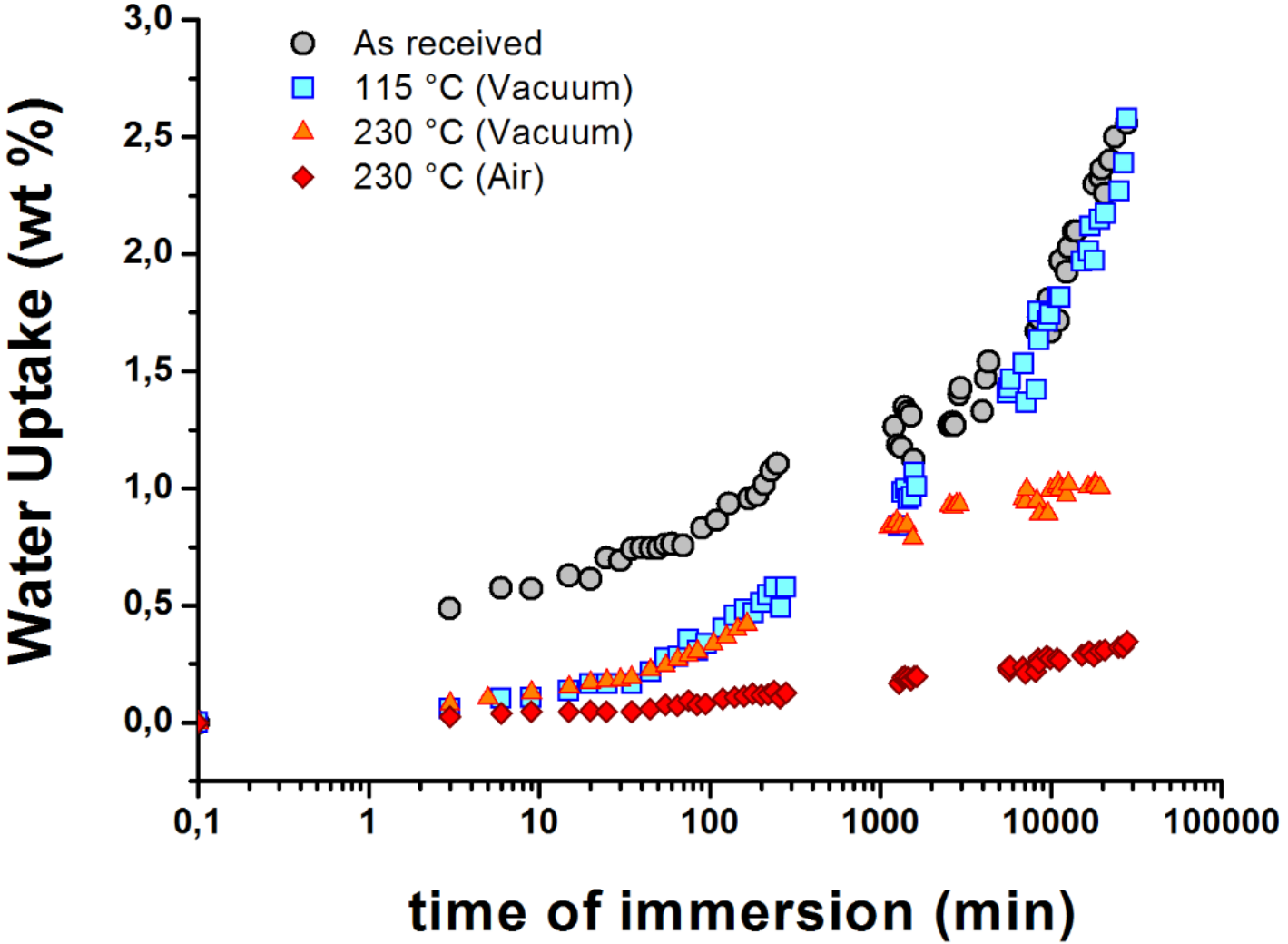
As received
115 °C (Vacuum)
230 °C (Vacuum)
230 °C (Air)
Water Uptake (wt %)
3,0
2,5
2,0
1,5
1,0
0,5
0,0
0,1
1
10
100
1000
10000
100000
time of immersion (min)

(a)

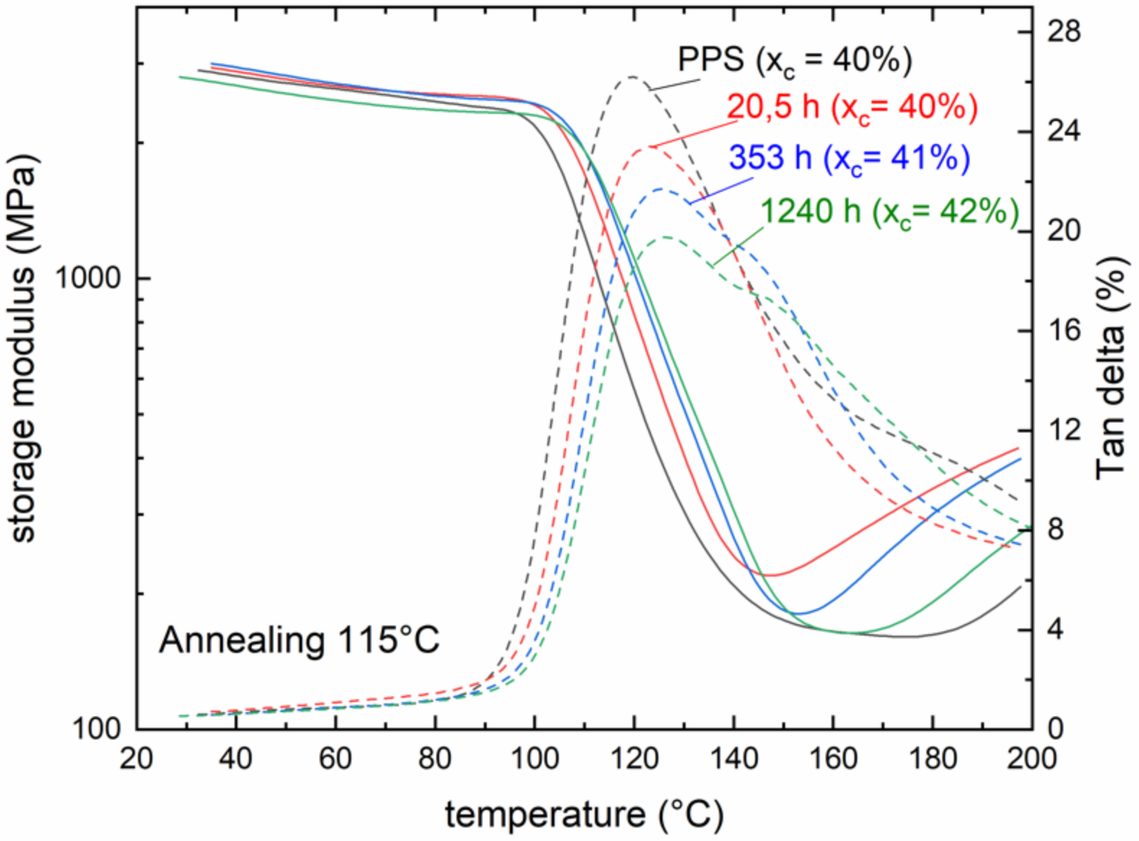
PPS (x_c = 40%)
20,5 h (x_c= 40%)
353 h (x_c= 41%)
1240 h (x_c= 42%)
Annealing 115°C
storage modulus (MPa)
Tan delta (%)
temperature (°C)
100
1000
20
40
60
80
100
120
140
160
180
200
0
4
8
12
16
20
24
28

(b)

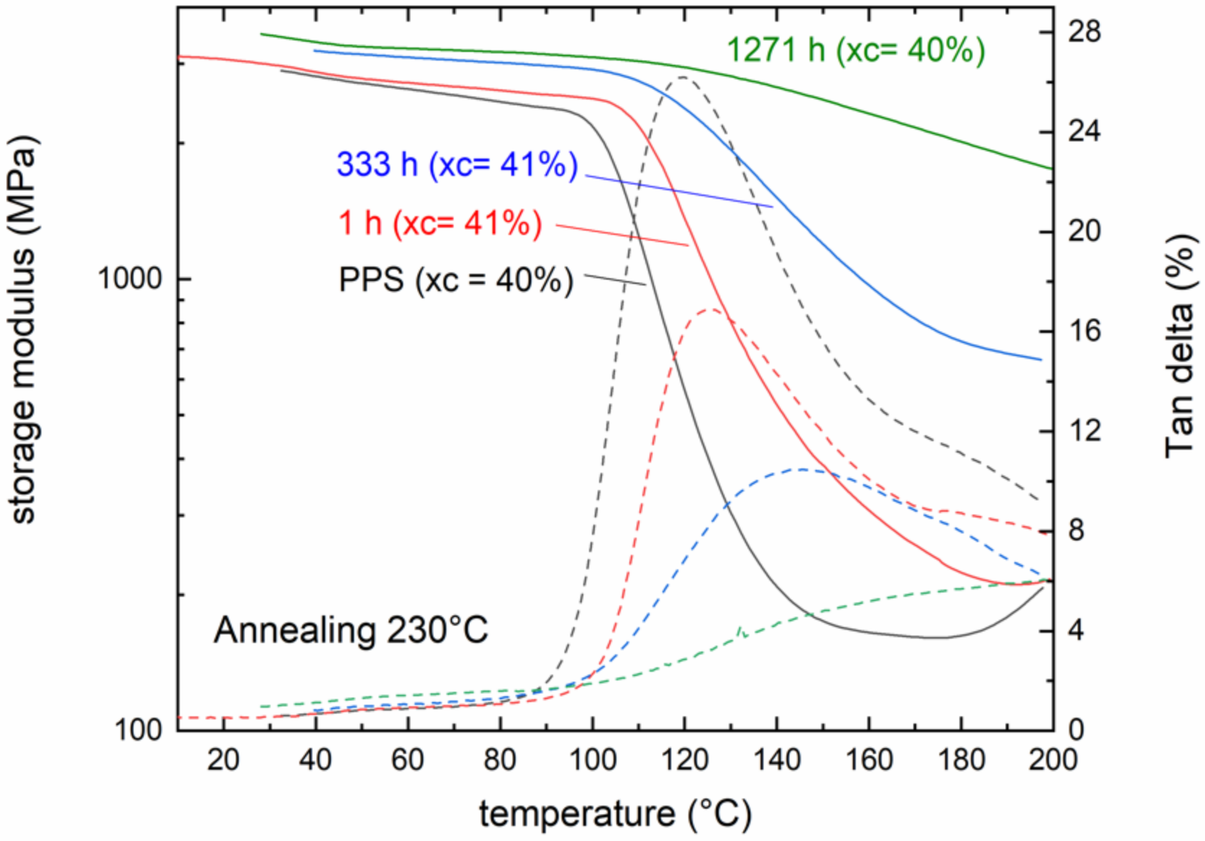
1271 h (xc= 40%)
333 h (xc= 41%)
1 h (xc= 41%)
PPS (xc = 40%)
Annealing 230°C
storage modulus (MPa)
Tan delta (%)
temperature (°C)
100
1000
20
40
60
80
100
120
140
160
180
200
0
4
8
12
16
20
24
28

(a)

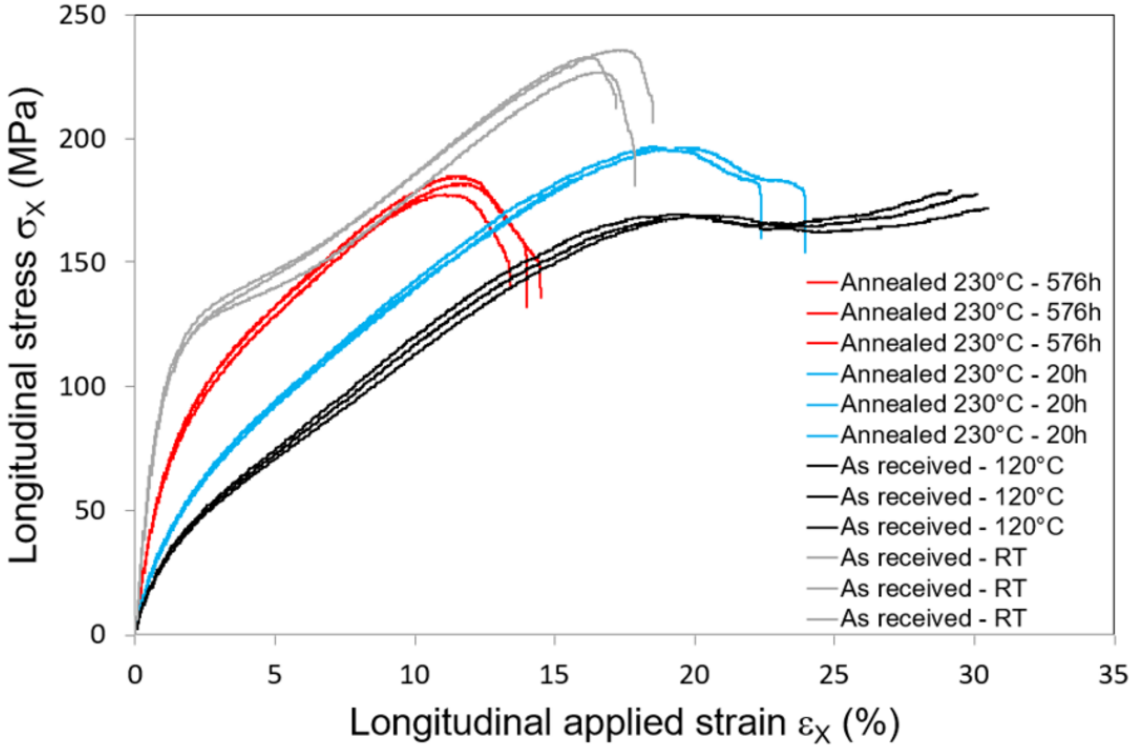
Longitudinal stress σX (MPa)
Longitudinal applied strain εX (%)
0
50
100
150
200
250
0
5
10
15
20
25
30
35
Annealed 230°C - 576h
Annealed 230°C - 576h
Annealed 230°C - 576h
Annealed 230°C - 20h
Annealed 230°C - 20h
Annealed 230°C - 20h
As received - 120°C
As received - 120°C
As received - 120°C
As received - RT
As received - RT
As received - RT

(b)

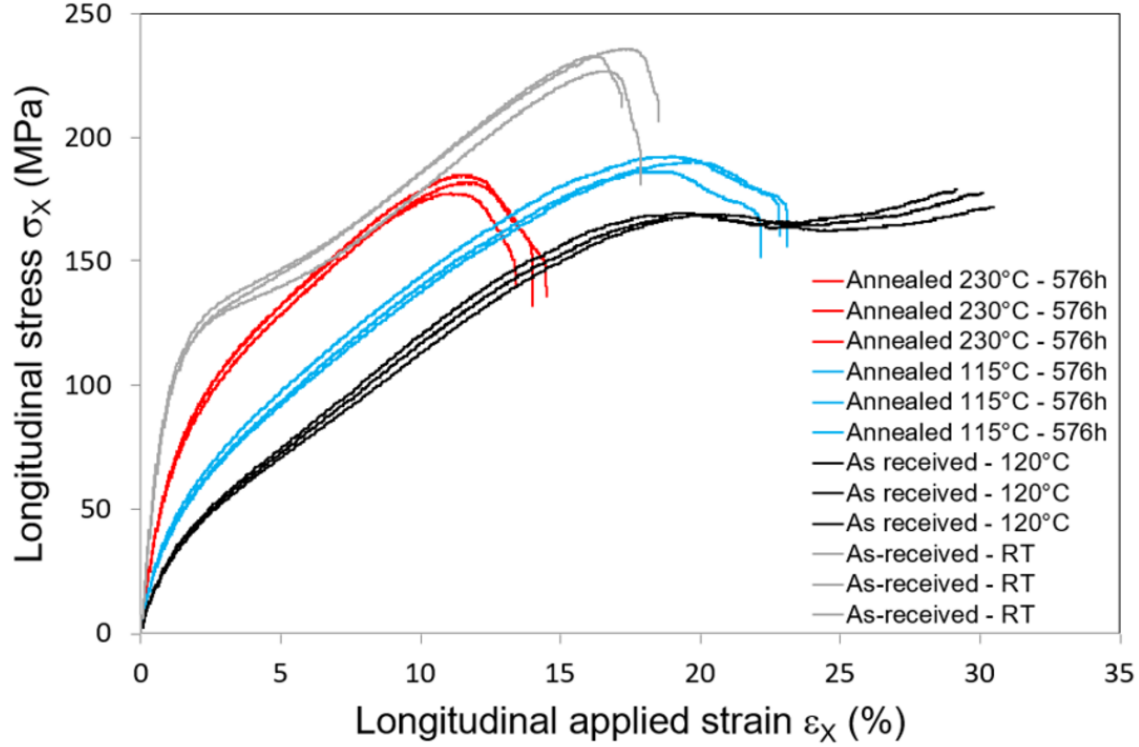
Longitudinal stress σX (MPa)
Longitudinal applied strain εX (%)
0
50
100
150
200
250
0
5
10
15
20
25
30
35
Annealed 230°C - 576h
Annealed 230°C - 576h
Annealed 230°C - 576h
Annealed 115°C - 576h
Annealed 115°C - 576h
Annealed 115°C - 576h
As received - 120°C
As received - 120°C
As received - 120°C
As-received - RT
As-received - RT
As-received - RT

(a)

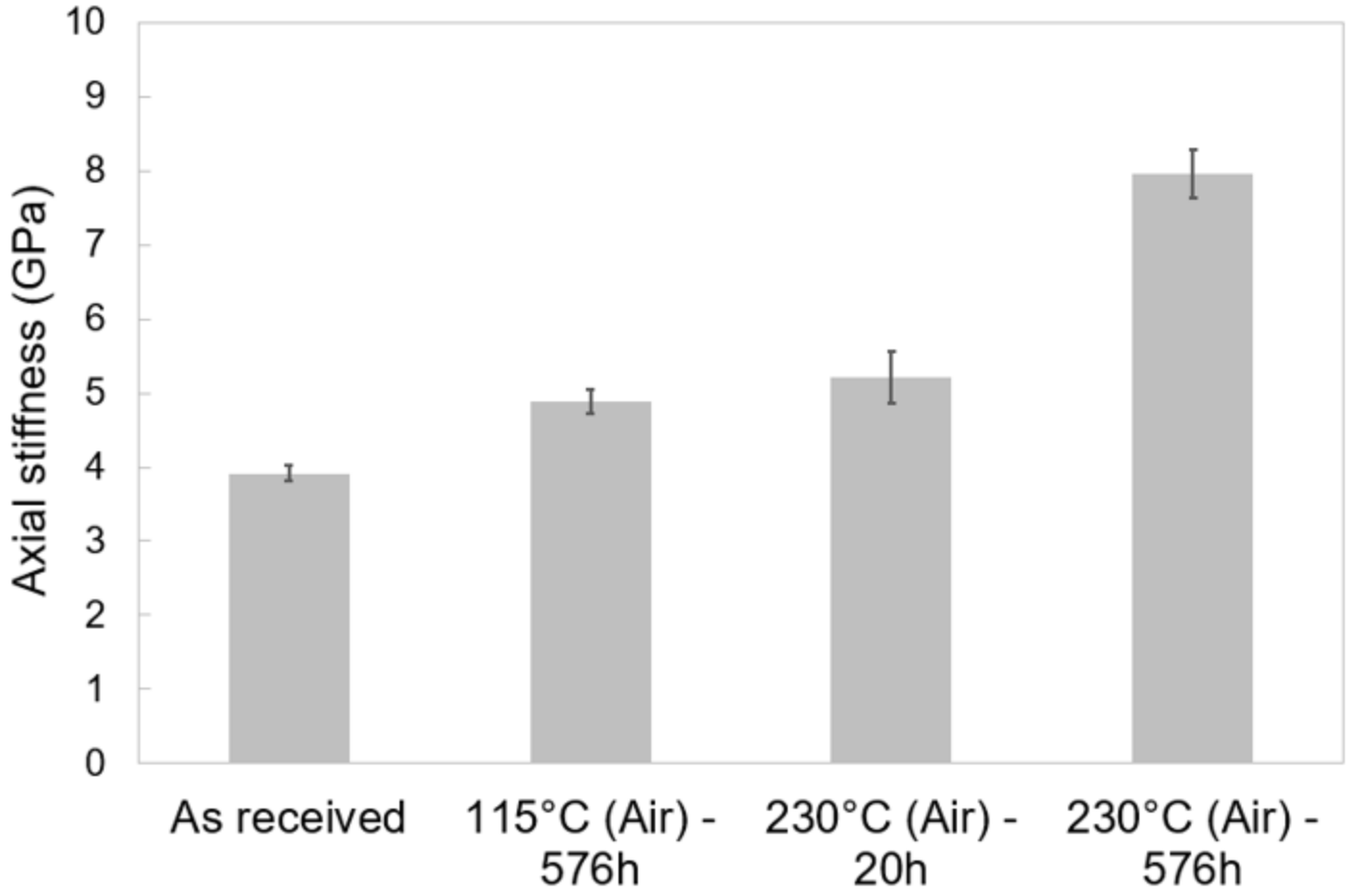
Axial stiffness (GPa)
0
1
2
3
4
5
6
7
8
9
10
As received
115°C (Air) - 576h
230°C (Air) - 20h
230°C (Air) - 576h

(b)

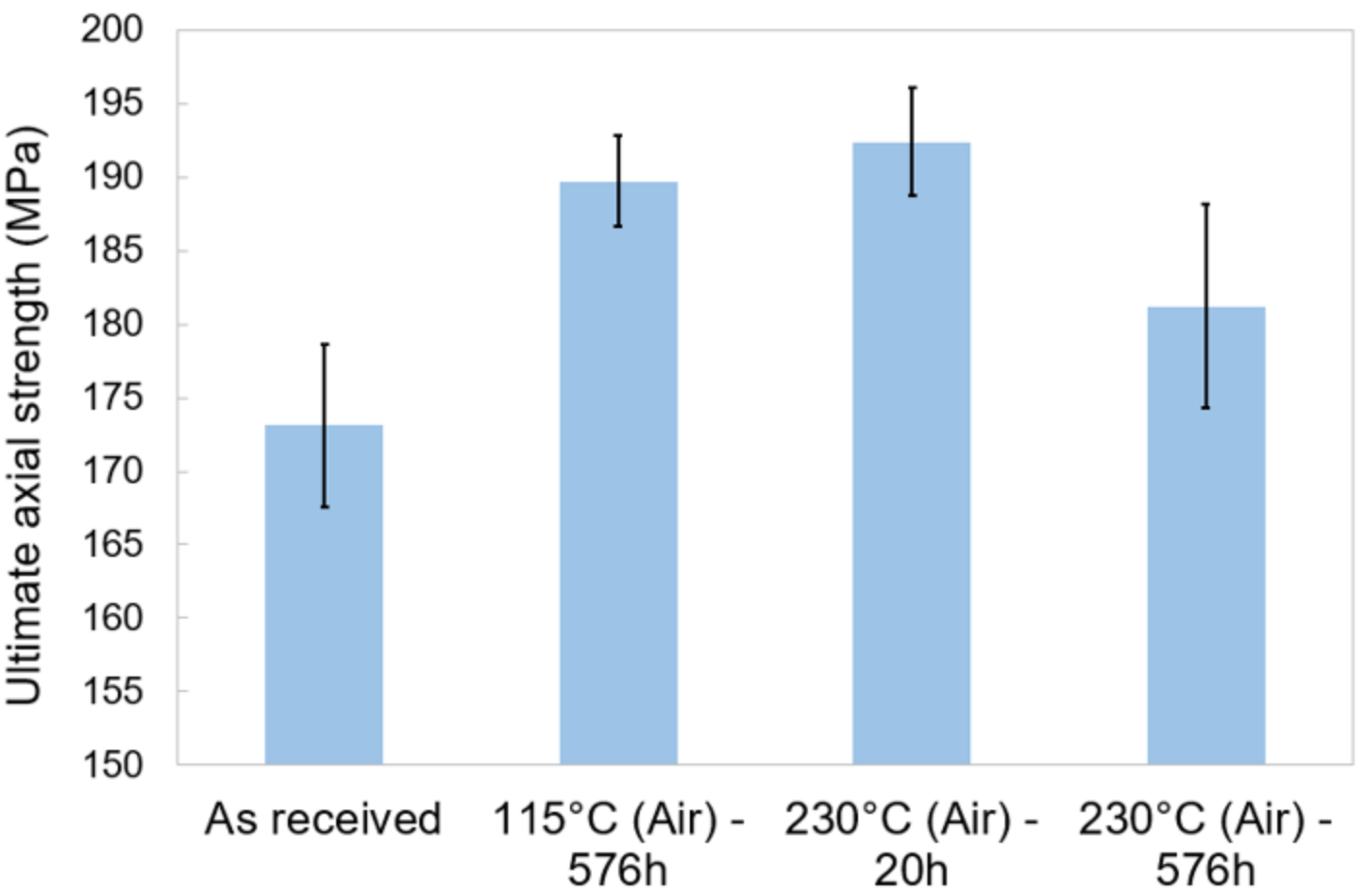
Ultimate axial strength (MPa)
150
155
160
165
170
175
180
185
190
195
200
As received
115°C (Air) - 576h
230°C (Air) - 20h
230°C (Air) - 576h

(c)

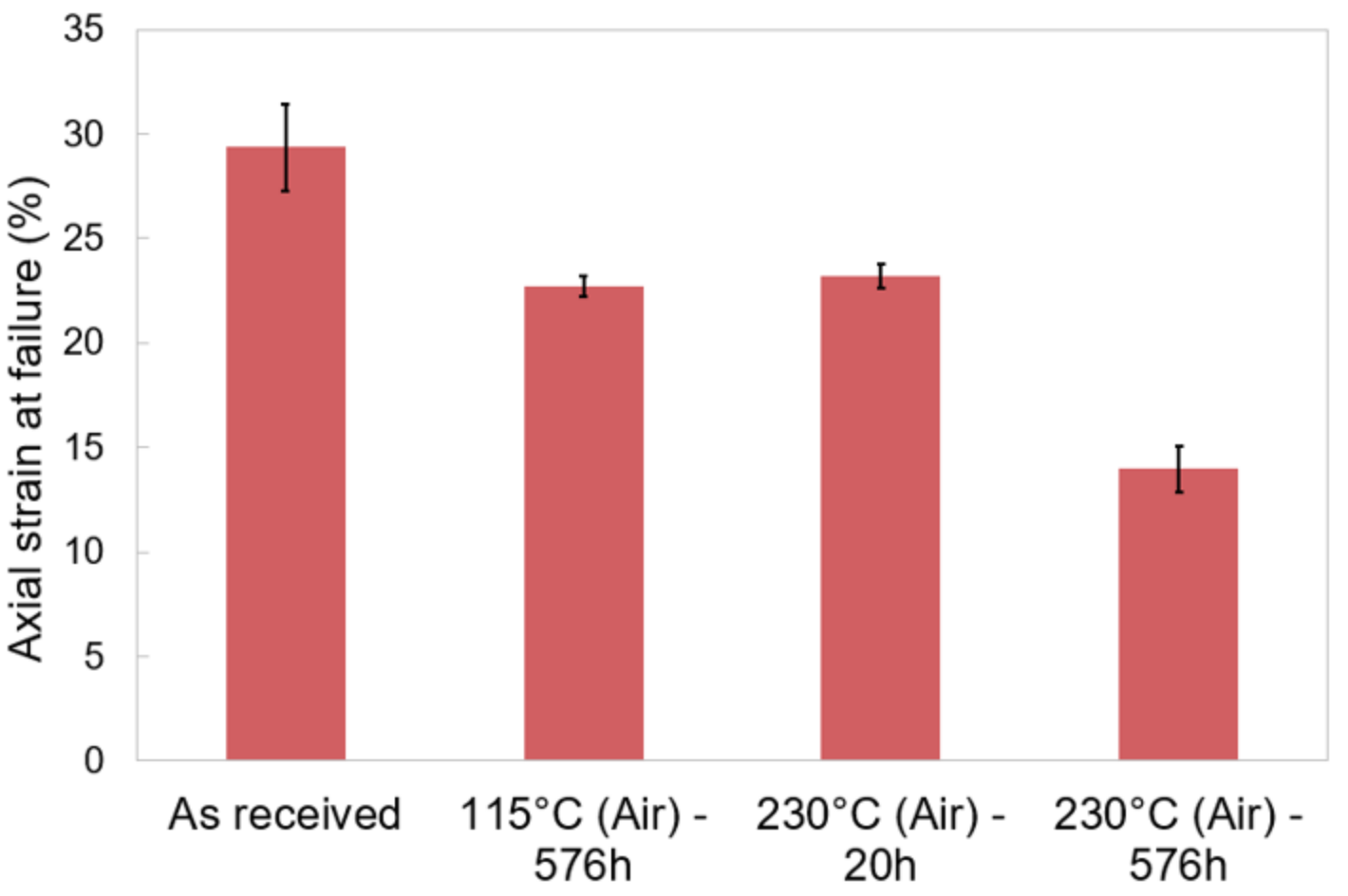
Axial strain at failure (%)
0
5
10
15
20
25
30
35
As received
115°C (Air) - 576h
230°C (Air) - 20h
230°C (Air) - 576h

(a) As received

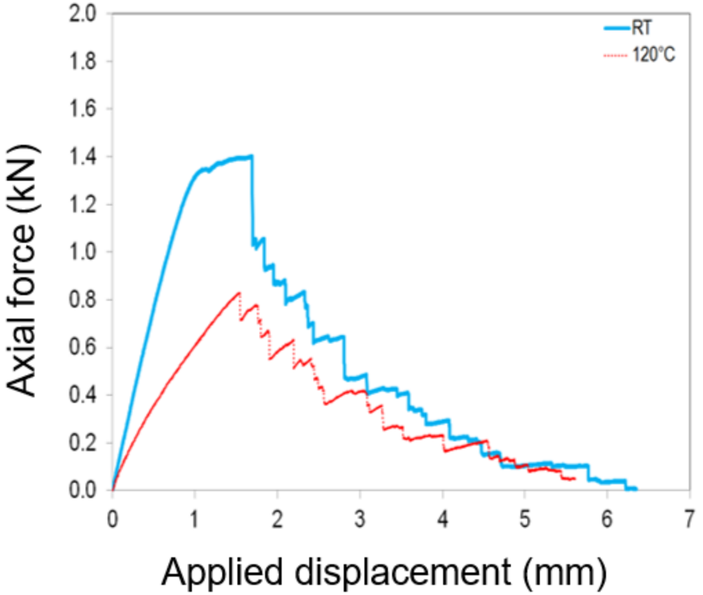

(b) Annealed at 115°C

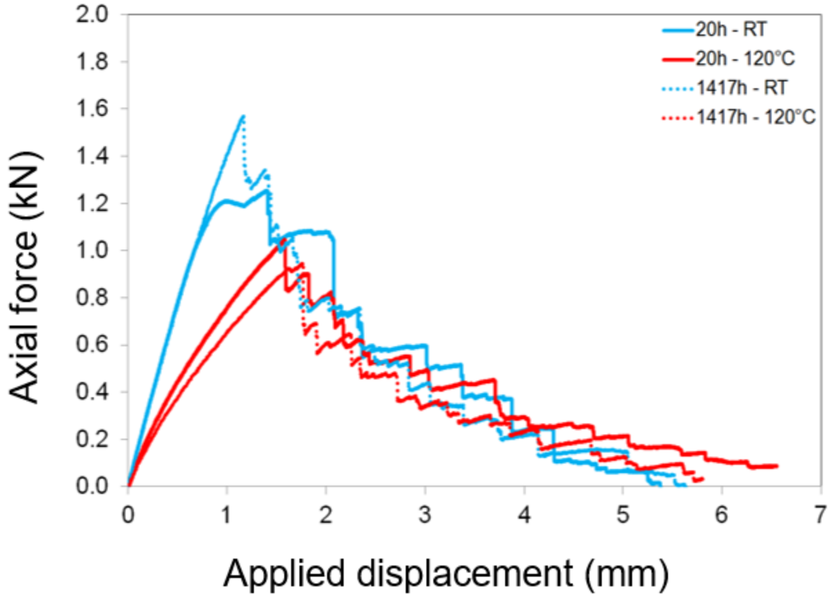

(c) Annealed at 230°C

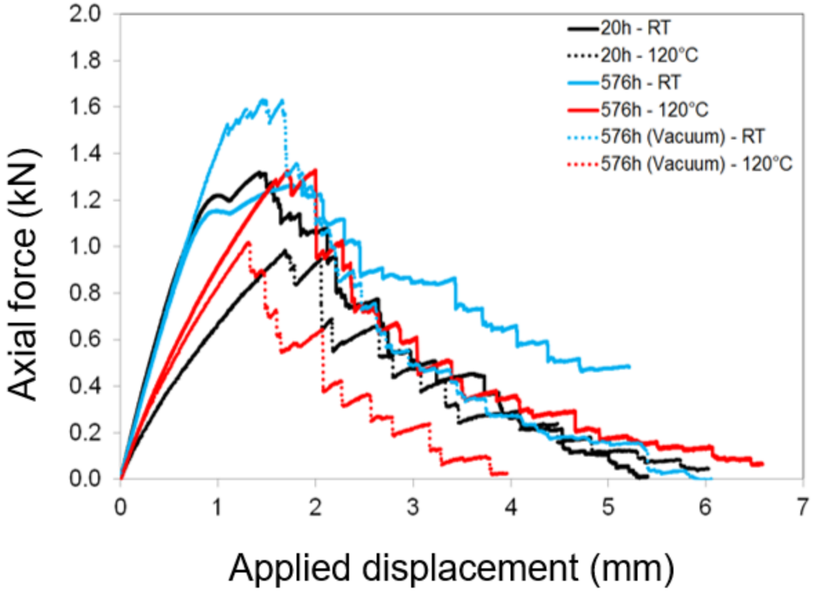

(a) Annealed at 115°C

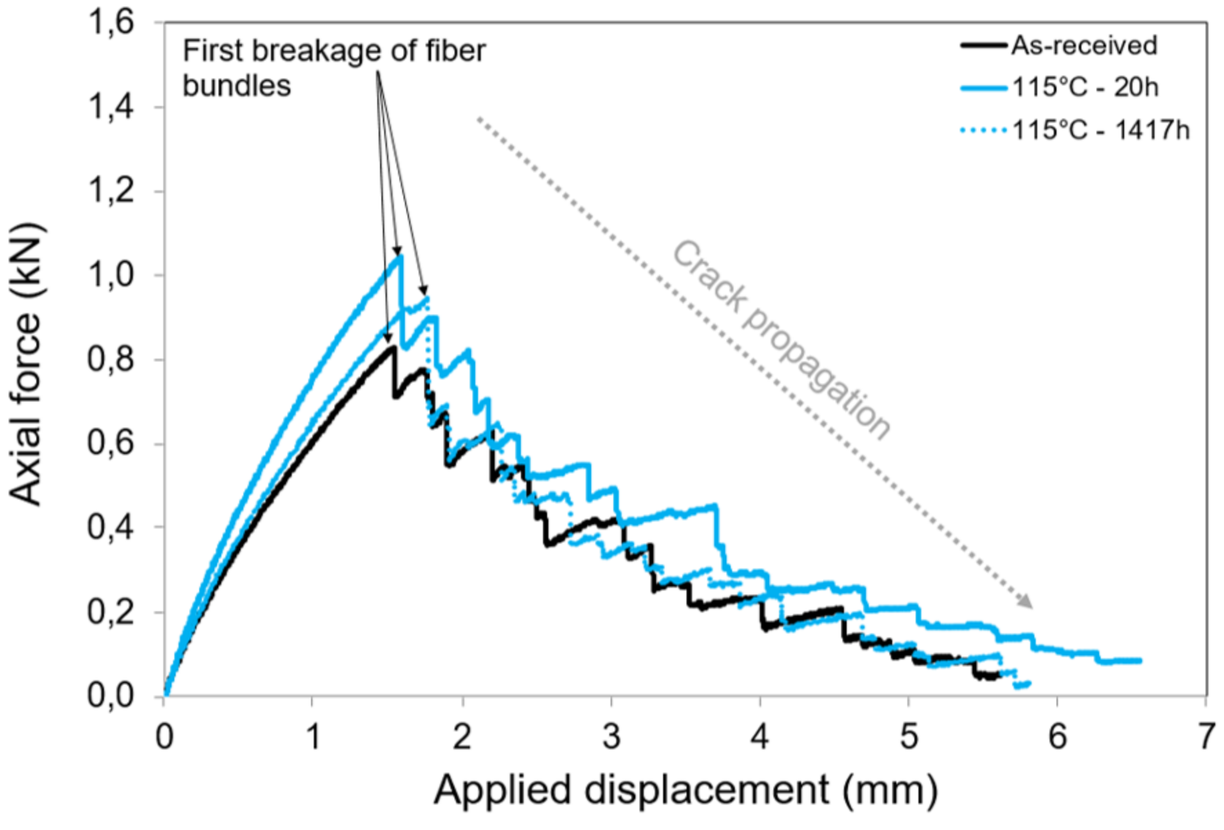

(b) Annealed at 230°C

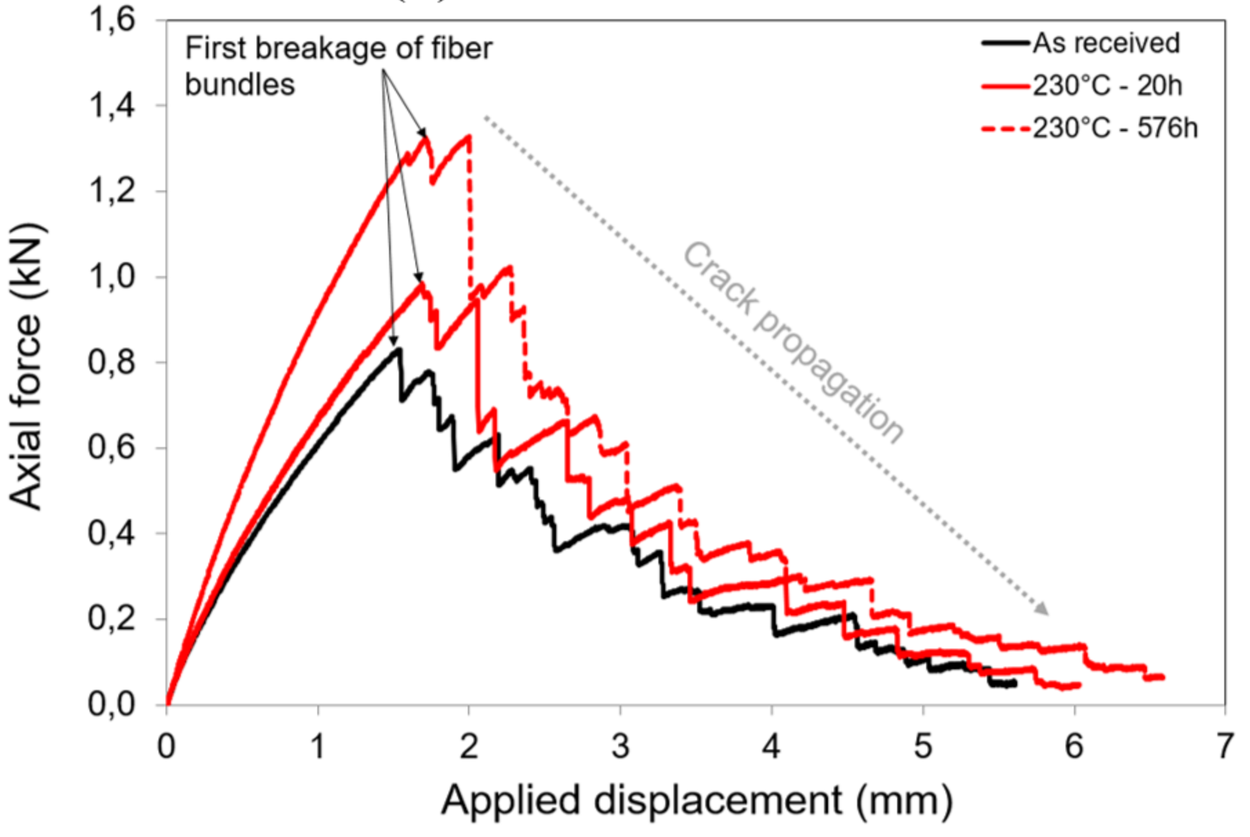

(a) Annealed for 20h under air

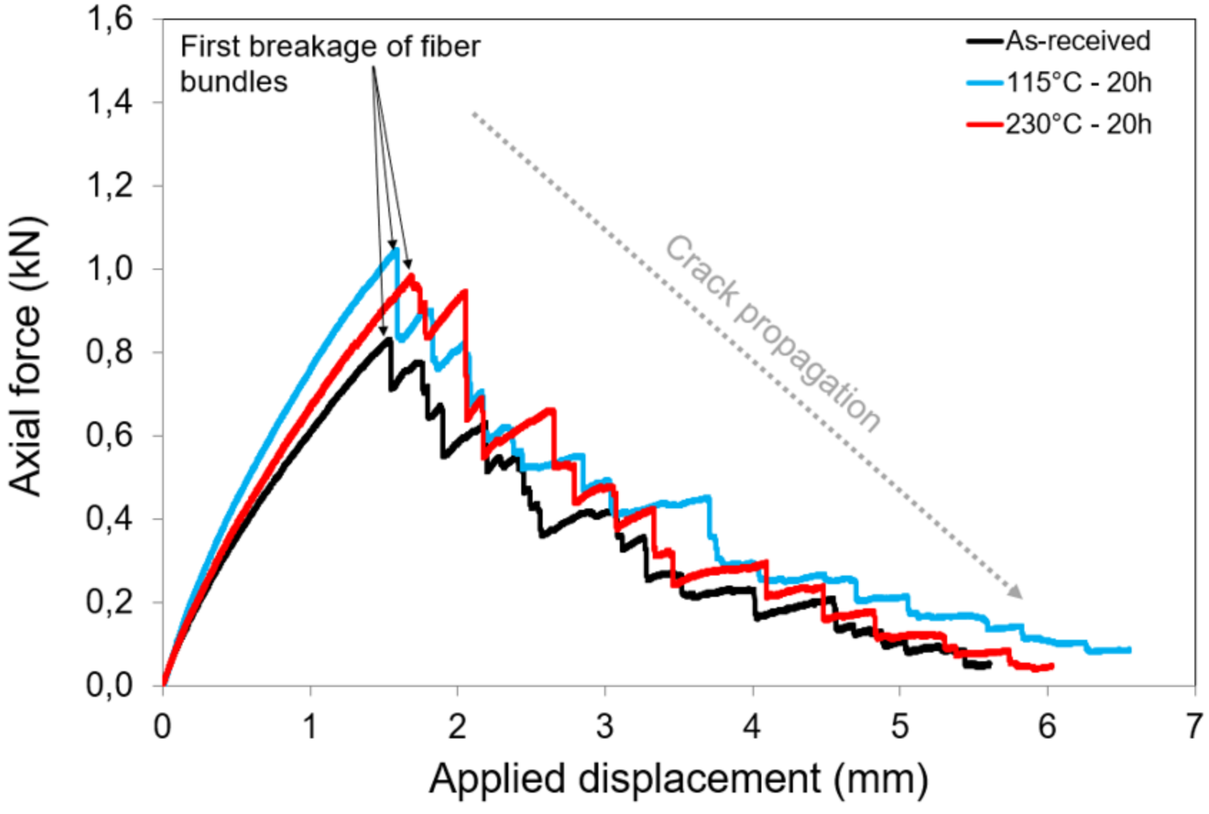

(b) Annealed for 576h at 230°C

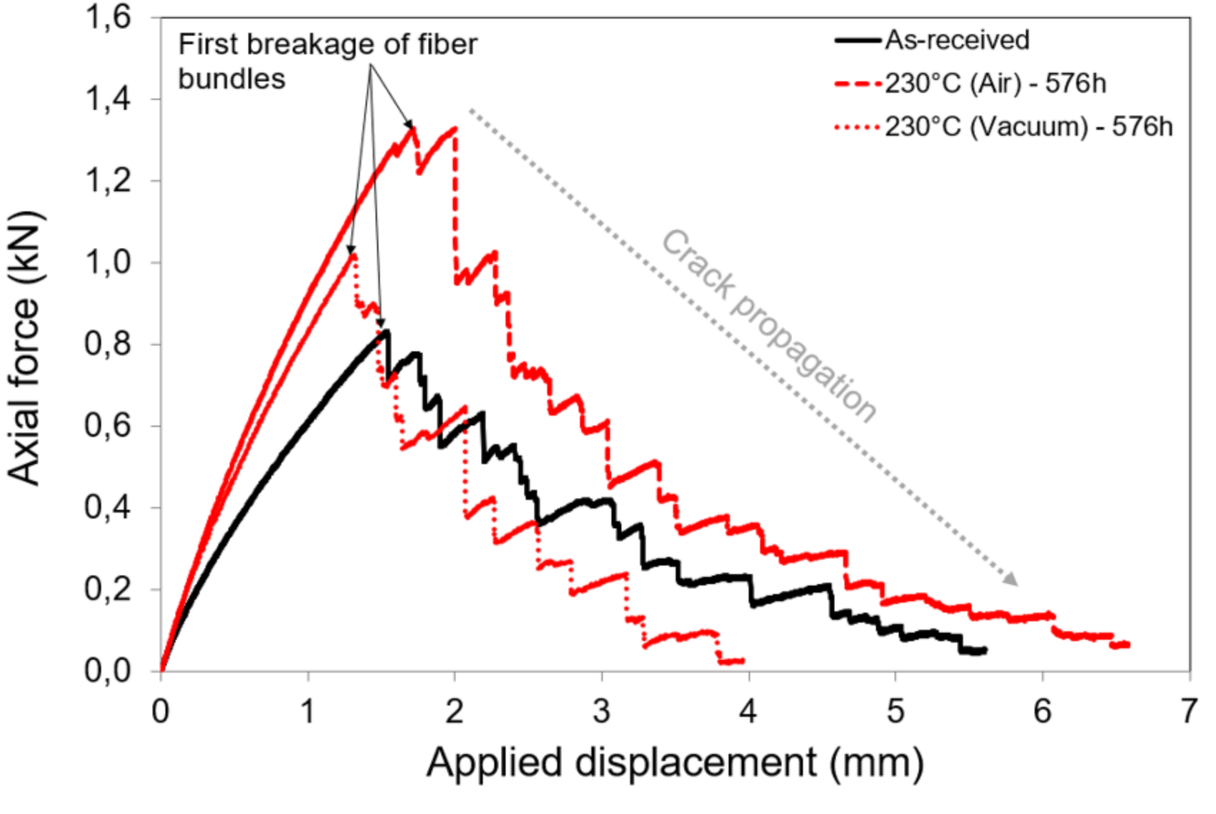

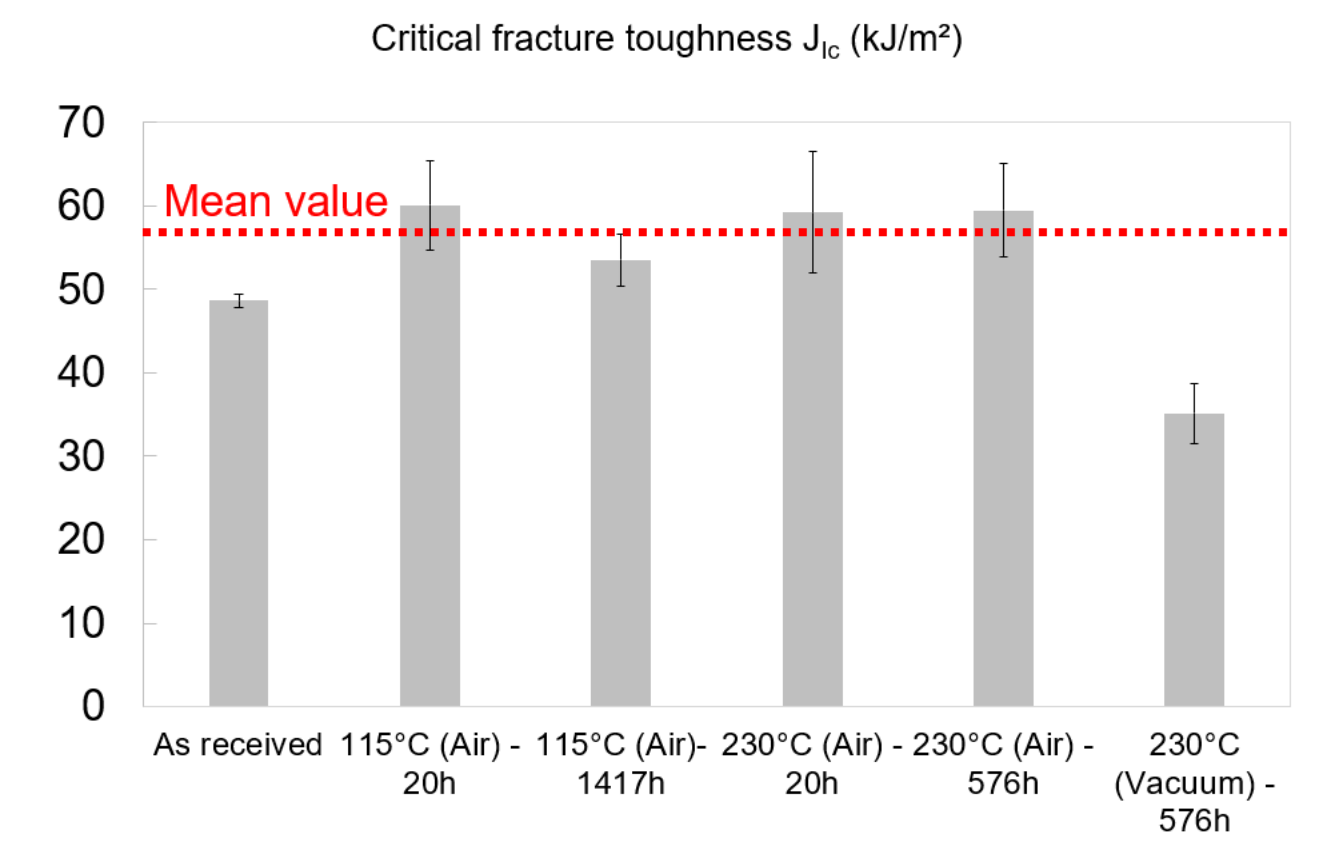
Critical fracture toughness J_{Ic} (kJ/m²)
70
60
50
40
30
20
10
0
Mean value
As received
115°C (Air) - 20h
115°C (Air)- 1417h
230°C (Air) - 20h
230°C (Air) - 576h
230°C (Vacuum) - 576h

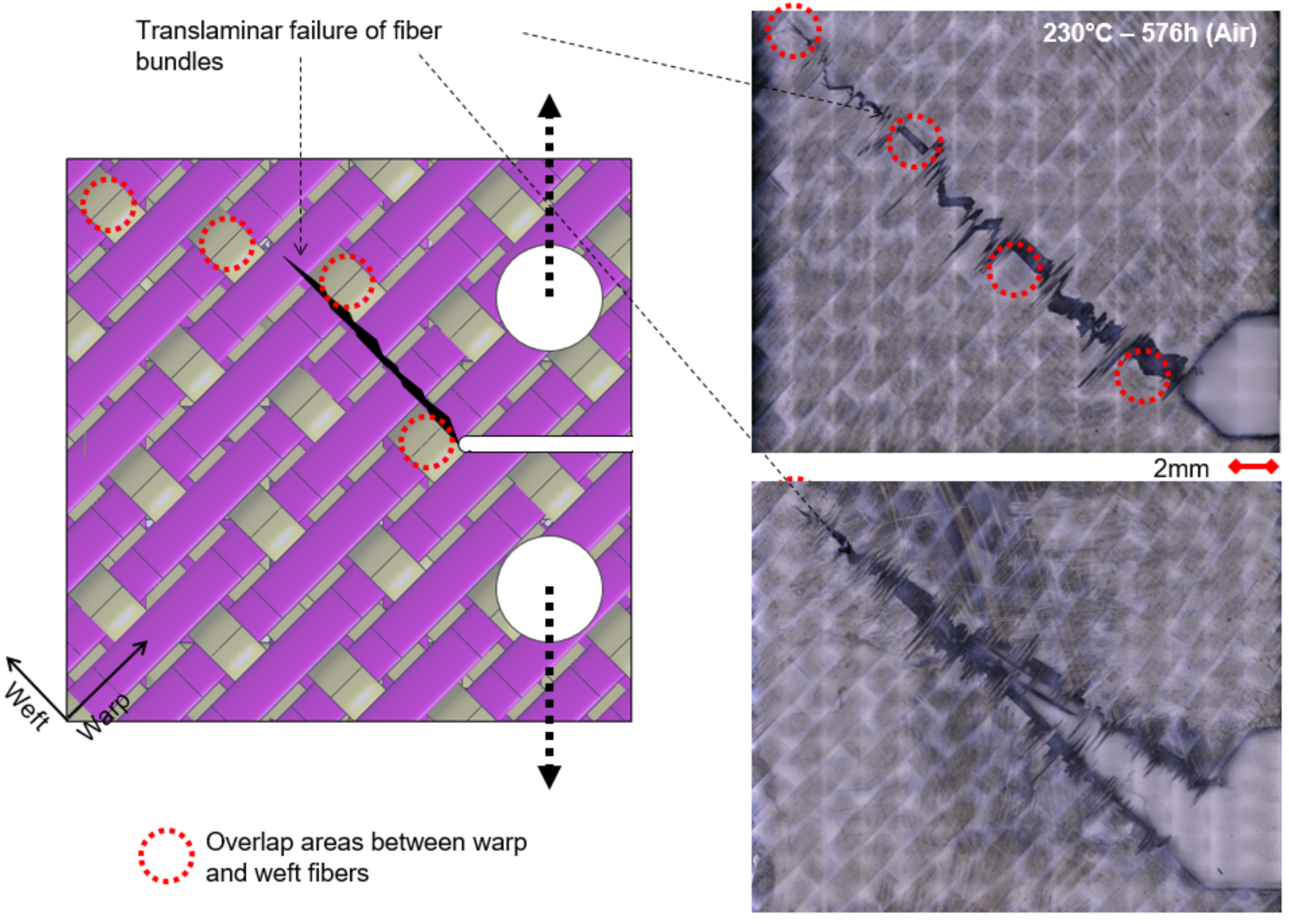
Translaminar failure of fiber bundles
230°C – 576h (Air)
2mm
Weft
Warp
Overlap areas between warp and weft fibers

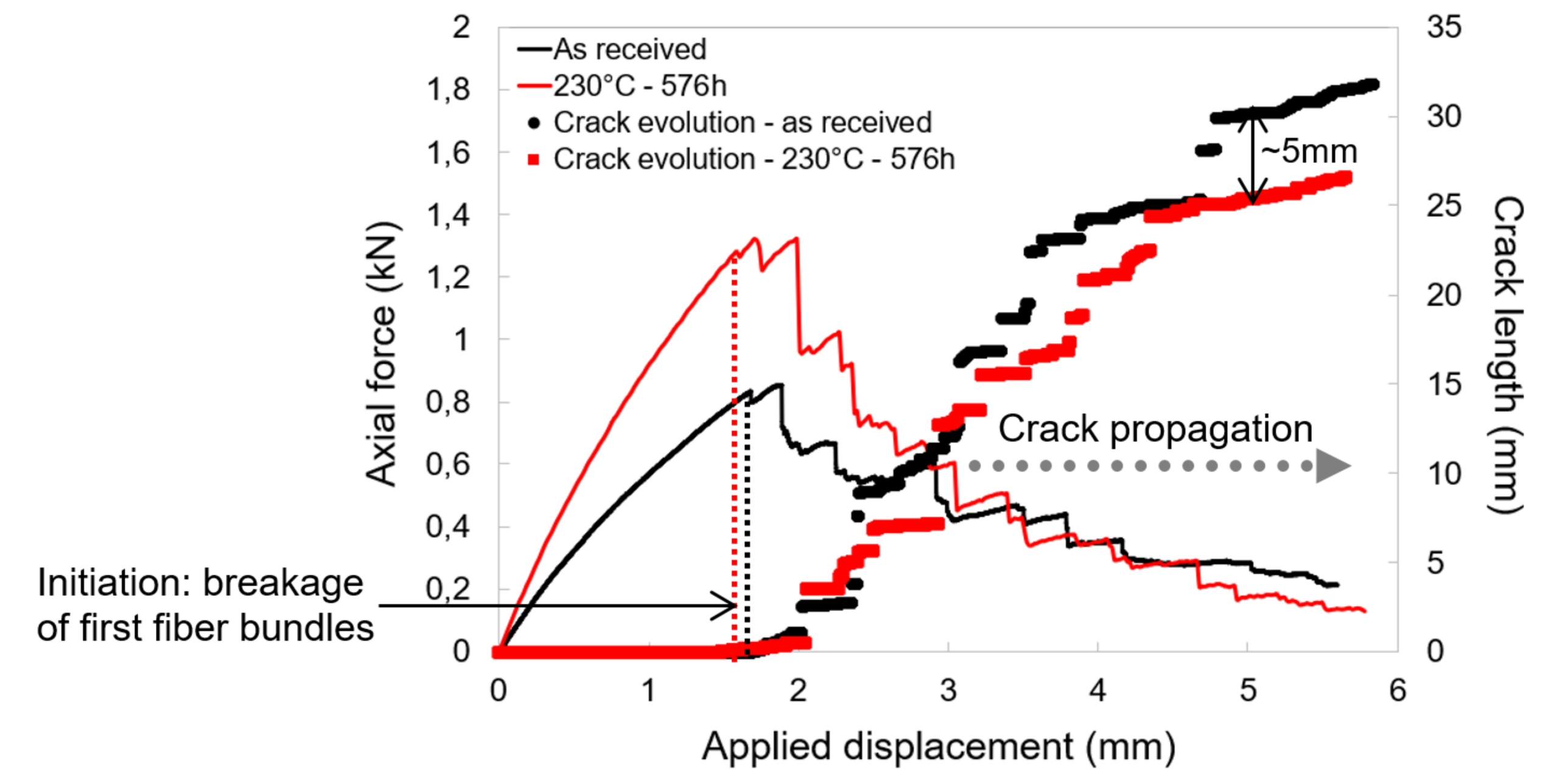
As received
230°C - 576h
Crack evolution - as received
Crack evolution - 230°C - 576h
~5mm
Crack propagation
Initiation: breakage of first fiber bundles
Axial force (kN)
Crack length (mm)
Applied displacement (mm)
0
0,2
0,4
0,6
0,8
1
1,2
1,4
1,6
1,8
2
0
5
10
15
20
25
30
35
0
1
2
3
4
5
6

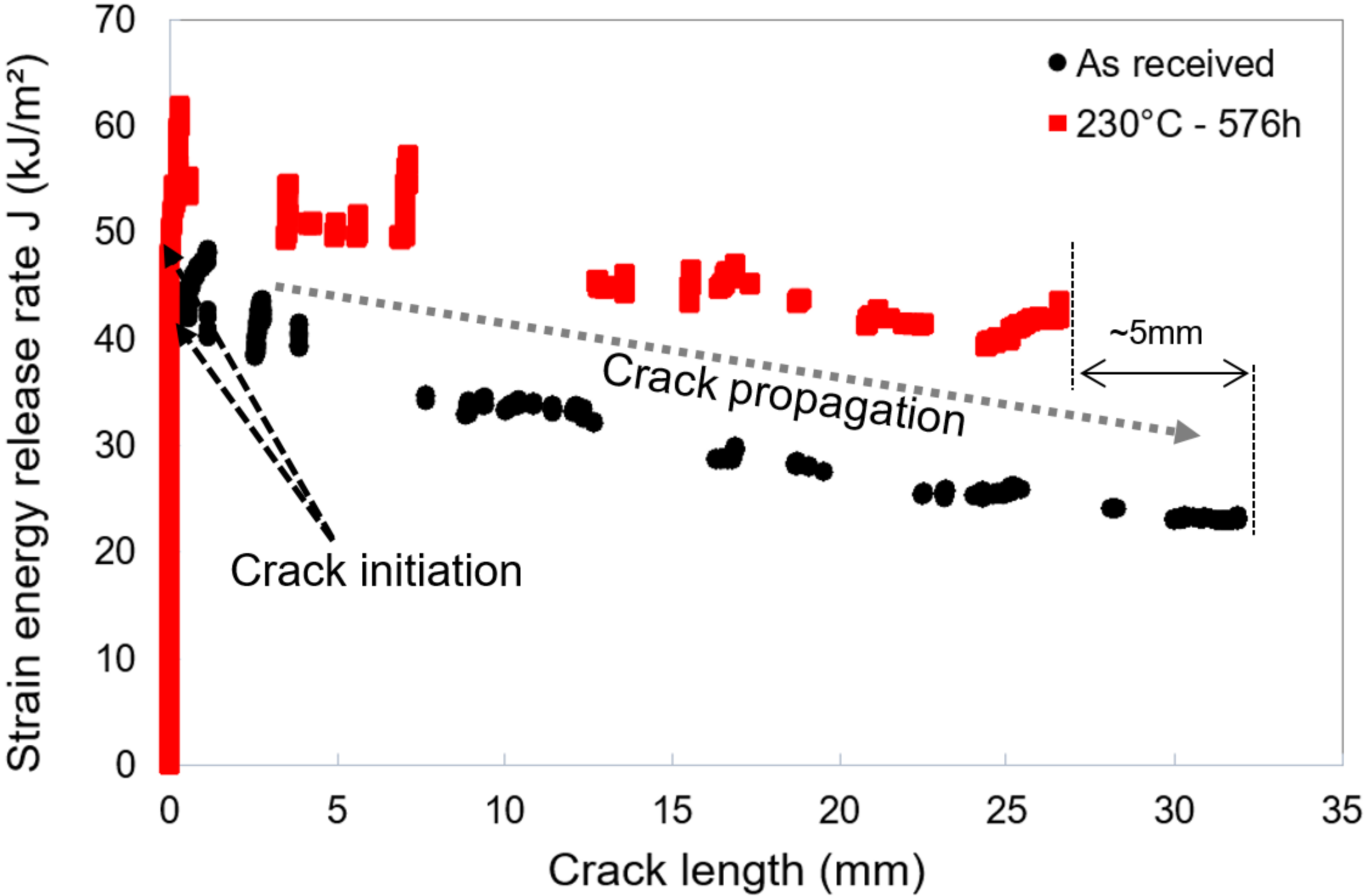
As received
230°C - 576h
Crack propagation
~5mm
Crack initiation
Strain energy release rate J (kJ/m²)
Crack length (mm)
0
10
20
30
40
50
60
70
0
5
10
15
20
25
30
35

Tables

	115°C - Air	230°C - Air	230°C - vacuum
Annealing time (h)	20-576-1417	20-576	20-576

Table 1 – Summary of the different annealing conditions